Highly anisotropic superconducting and normal-state properties of Sr_2RuO_4

Koji Yoshida

Department of Physics, Faculty of Science, Hiroshima University

1-3-1 Kagamiyama, Higashi-Hiroshima 739, Japan

Abstract

We have recently discovered superconductivity of Sr_2RuO_4 with $T_c \approx 1$ K. This compound is the only layered perovskite superconductor without copper that is known so far: the same crystal structure as a high-T_c superconducting copper oxide. In this study, we have investigated the superconducting and normal-state properties of Sr_2RuO_4 by measuring the electrical resistivity, magnetic susceptibility and specific heat using single crystals.

In the normal state we found the T^2 dependence of the resistivity below 25 K, the enhanced paramagnetic spin susceptibility, and the enhanced Sommerfeld coefficient of the specific heat. These three results can consistently be described as a highly-anisotropic Fermi-liquid behavior of the normal state of Sr_2RuO_4. In addition, concerning the peculiar temperature dependence of the resistivity along the c axis, we present a systematic interpretation based on competition between the life time of the quasiparticles governed by a number of scattering processes and the time for the quasiparticles to travel the interlayer distance d.

From the upper critical fields H_{c2}, we will show that the superconducting state of Sr_2RuO_4 is also highly anisotropic with the ratio of the coherence lengths $\Gamma_S = \xi_{ab}(0)/\xi_c(0) = 26$ evaluated for zero temperature. Furthermore, we found peculiar anisotropic flux-pinning behavior: a second dissipation peak in the ac susceptibility prominently appears only when the direction of the flux lines, as well as of their induced motions, is parallel to the ab planes. The peak effect in Sr_2RuO_4 is attributed to the synchronization of the flux lines to the pinning centers as the flux-line lattice softens with increasing magnetic field and temperature.

In this study we clarify that Sr_2RuO_4 serves as an ideal reference material for investigation of the limits of applicability of the Fermi liquid theory to other highly correlated layered compounds, including high-T_c cuprates. In addition, the comparison with these physical properties of Sr_2RuO_4 and those of high-T_c superconductors are very important to clarify the mechanism of the high T_c, which still remains unclear at present.

Contents

1. Introduction

Since the discovery of high-T_c superconductors (HTSC) [1], active investigations continue to clarify the mechanism of the high-T_c superconductivity. However, the origin of the high-T_c superconductivity still remains unclear. The formation of the Cooper pairs cannot be explained at least by a simple *s*-wave coupling originating from conventional electron-phonon interactions. One of the key characteristics of HTSC is the quasi-two dimensionality attributed to the conductive planes of CuO_2, the key elements of the layered perovskite structure. The superconductivity appears by carrier doping into the CuO_2 planes of the parent compounds, which are Mott-Hubbard insulators owing to the strong Coulomb interactions among the electrons. An example of the parent compound is La_2CuO_4, for which $La_{2-x}Sr_xCuO_4$ exhibits the superconductivity with $T_c \leq 40$ K. In addition, the fact that no superconductor exists in a variety of layered perovskite compounds without copper had suggested that the special electronic state of the CuO_2 planes is responsible not only for the high T_c, but also for the appearance of the superconductivity itself.

We discovered, however, a year and a half ago that Sr_2RuO_4 is the first layered perovskite superconductor ($T_c \approx 1$ K) without copper [2]. The variations of the resistivity and ac susceptibility with temperature are shown in Fig. 1. The crystal structure is of the same K_2NiF_4-type as a typical HTSC, $La_{2-x}Sr_xCuO_4$, containing quasi-two-dimensional conductive planes of RuO_2, as depicted in Fig. 2. This indicates that the two-dimensional electronic state of the CuO_2 planes is not always required for the appearance of superconductivity in the layered perovskite oxides. Therefore, it is very important to investigate the differences, as well as the similarities, between the physical properties of Sr_2RuO_4 and those of HTSC in order to help clarifying the mechanism of the high T_c.

Let us compare the basic electronic states of Sr_2RuO_4 and $La_{2-x}Sr_xCuO_4$. The ionic state of Ru in Sr_2RuO_4 is Ru^{4+} in the $4d^4$ (t_{2g}^4) electron configuration in the low spin state [3] with spin quantum number $S = 1$. This is compared with Cu^{2+} in $3d^9$ ($t_{2g}^6 e_g^3$) configuration with $S = 1/2$ in La_2CuO_4. It should be noted that the electronic states at the Fermi level in Sr_2RuO_4 consist of hybridized orbitals of Ru 4*d* and O 2*p* electrons ($pd\pi^*$ anti-bonding orbitals) [4], analogous to those of Cu 3*d* and O 2*p* in HTSC ($pd\sigma^*$ anti-bonding orbitals). Experiments on quantum oscillations in the normal state of Sr_2RuO_4 indicated three nearly cylindrical sheets of Fermi surfaces with slight dispersion along the *c* axis [5]. Similarly the band calculations [4] predicted three Fermi surfaces, two of which are electron-like and the other is hole-like. These electronic

states of the RuO_2 planes must be important as the stage for the superconductivity in Sr_2RuO_4. It should be noted that Sr_2RuO_4 is intrinsically metallic without acquired carrier doping, in contrast to La_2CuO_4. Although the band calculations [6] predict that La_2CuO_4 is a metal with a single cylindrical Fermi surface, it is actually an insulator because of the strong electronic correlations, which are not properly taken into account in the band structure calculations. Despite the similar Fermi surfaces of the experimental results and the band calculations for Sr_2RuO_4, this ruthenate is possibly in the vicinity of the Mott-Hubbard insulators, because the photoemission spectra [7] clearly indicate the formation of the lower Hubbard band owing to the electron correlations. Therefore, Sr_2RuO_4 has key components in its basic electronic structure, which are considered essential for the understanding of the high-T_c superconductivity.

Not only the high T_c but also the peculiar metallic behavior in the normal state [8] and the unique vortex phases in the mixed state [9] distinguish HTSC from conventional superconductors. The resistivity along the *ab* planes shows the linear dependence on temperature over a quite wide temperature range from just above T_c to a temperature higher than the Debye temperature [10, 11]. This behavior can not simply be explained in terms of the electron-phonon scattering. The peculiar scattering mechanisms, for example that based on the scattering of charge carriers due to spin fluctuation [11] has been discussed. It is believed that this unusual resistivitive properties reflect the peculiar electronic states generating the high-T_c superconductivity.

A recent controversy is whether the ground state of HTSC after suppressing the high-T_c superconductivity is a Fermi liquid. The Fermi liquid theory has been helpful to explain the normal-state properties of HTSC in the heavily over-doped region, where the superconductivity does not appear. However, for $Tl_2Ba_2CuO_{6+\delta}$ ($T_c < 15$ K), which is the material near the over-doped regime, the strong temperature-linear term in the resistivity along the *ab* planes survives even down to millikelvin temperatures under a magnetic field of 16 T (// *c*) [12], in contrast to the T^2 dependence predicted for a Fermi liquid.

Another controversy is whether a non-metallic conduction appears along all crystalline direction at low temperatures in HTSC in the underdoped regime when the high-T_c superconductivity is suppressed. The resistivity along both the *ab* plane and the *c* axis of $La_{2-x}Sr_xCuO_4$ with $x = 0.08$ and 0.13 under high magnetic fields $\mu_0 H$ of 61 T, by which T_c is suppressed to less than 1 K, shows the non-metallic behavior over a wide range of temperatures below $T_c(H = 0$ T); it seems to diverge as $\ln(1/T)$ as T approaches the absolute zero [13]. On the other hand, in $YBa_2Cu_{3-x}Zn_xO_7$ although the resistivity along the *c* axis is non-metallic at low

temperatures, that along the *ab* planes remains metallic [14]. The localization in the *c* direction alone is inconsistent with the general scaling theory of disordered systems. This behavior is probably attributable to the confinement of the carriers within the *ab* planes [14, 15].

It is also quite important to clarify the mechanism of the anomalous flux pinning of high-T_c cuprate superconductors (HTSC), because the complex magnetic phase diagram of the mixed state may be intimately related to the basic nature of high T_c itself. Among a variety of peculiarities of the mixed state are the peak effect and the loss of irreversibility of flux lattice in a particular *H-T* region. The former refers to the presence of a peak in the critical current as a function of magnetic field or temperature, or to the associated peak in the energy dissipation. The peak effect often reflects a changeover in the pinning mechanism within the mixed state. The corresponding *H-T* lines in the magnetic phase diagram depend only on the component of the dc magnetic field parallel to the *c* axis which is normal to the CuO_2 planes. This anisotropic behavior has been frequently interpreted as an evidence for unusual two-dimensional vortices, namely pancake vortices [16], originating from the highly anisotropic superconducting state which reflects the layered structures of HTSC.

Given the structural and electronic analogy with the cuprate superconductors, and the fact that Sr_2RuO_4 is the only layered-perovskite superconductor without copper that is known so far, the understanding of the superconducting, normal-state and vortex-state properties of high quality single crystals is of great interest in clarifying the connections to the cuprates. In the present work, we investigated the dc-susceptibility and specific heat above T_c, as well as the resistivity and the ac-susceptibility under magnetic fields below 2 K, using single crystalline Sr_2RuO_4. We observed the quadratic temperature dependence of resistivity, the enhanced magnetic susceptibility which is nearly temperature independent, and linear temperature dependence of the specific heat with the enhanced Sommerfeld constant (Sec. 3.1). Based on these results, we will show in Sec. 3.2 that the normal state of Sr_2RuO_4 is described very well as an anisotropic Fermi liquid with a nearly two-dimensional electronic character of the RuO_2 planes. The resistivity along the *c* axis of Sr_2RuO_4 exhibits a crossover at T_M = 130 K from the metallic to non-metallic temperature dependence with decreasing temperature. In Sec. 3.3, we will quantitatively explain this peculiar phenomenon in terms of relaxation times of the quasiparticles for a number of scattering processes.

The investigation of the upper critical fields H_{c2} shows that the superconducting state of Sr_2RuO_4 is also highly anisotropic with the ratio of the coherence lengths $\Gamma_S = \xi_{ab}(0)/\xi_c(0) = 26$ evaluated for zero temperature (Sec. 4.1.1). We present the superconducting parameters

evaluated from H_{c2} and T_c (Sec. 4.1.2). We also report peculiar anisotropic properties of flux pinning (Sec. 4.2). We will extensively discuss a second dissipation peak which was found at low fields only when H_{dc} is applied parallel to the *ab* planes in Sec. 4.2.5.

2. Experimental

2.1 Sample preparation

The crystals used were grown by a floating-zone method similar to that reported previously [17]. The starting materials were $SrCO_3$ with a purity of 99.99 % and RuO_2 with that of 99.9 %. They were weighed in the molar ratio of Sr : Ru = 2 : 1.1. The excess Ru is added because of the high vapor pressure of Ru at high temperature during the crystal growth. The powders were ground in a dry nitrogen atmosphere and the mixture was prereacted in air at 900 ℃ and 1150 ℃ for a total of 48 hr with intermediate grindings. After being pressed into a rod with a diameter of 6 mm, it was sintered in air at 1350 ℃ for 4 hr. The rod was then set in a floating-zone furnace (Nichiden Machinery : SC-15HS-M). The growth of the crystals was performed in air at the feed speed of 20 mm/hr. The rod and crystal seed were oppositely rotated each other at 30 rpm.

The grown crystals were easily cleaved, so we obtained plate-like crystals. From X-ray Laue diffraction, it was found that the planar surface is the (001) plane. A typical size of the crystals used in ac susceptibility measurements is (2× 2× 0.5) mm^3, with the shortest dimension along the *c* axis. Powder X-ray diffraction of crashed crystals at room temperature did not detect any impurity peaks and is consistent with the tetragonal K_2NiF_4-type structure with $a = b = 3.87$ Å and $c = 12.74$ Å. The samples exhibit a T_c of ≈ 1 K with a transition width of ~ 0.1 K. The crystals used in this study are taken from the same crystal rod used for quantum oscillation measurements [5].

2.2 Measurements

The resistivity was measured using a standard four probe method. A silver paste (Dupont, 6838) is used for attaching electrocodes and is cured in air at 500 ℃ for 5 min [18]. This process does not affect the oxygen stoichiometry [19] and results in a strong reduction in the contact resistance: we attained the contact resistance of < 0.5 Ω. This low contact resistance is important to achieve the homogeneous current paths within the sample. Measurements of the magnetic susceptibility of the normal state were performed between 5 and 700 K with a constant field of 1

T by using a SQUID magnetometer. The magnitude of the magnetic fields was precisely calibrated using the standard sample of Pd. The specific heat measurements were performed by a conventional adiabatic method using a ^{4}He cryostat with a mechanical switch. The ac susceptibility (χ', χ'') was measured by a mutual-inductance method under dc fields $\mu_0 H_{dc}$ up to 8 T, using a commercial dilution and ^{3}He refrigerators.

3. Normal-State Properties

In this chapter, we will first show the Fermi-liquid behavior in the resistivity, magnetic susceptibility and specific heat. We will then discuss how these results are interrelated to describe coherently the anisotropic Fermi-liquid behavior of Sr_2RuO_4 [20]. In addition, we discuss the observed peculiar temperature dependence of the resistivity along the c axis.

3.1 Experimental results

3.1.1 Resistivity

The variations of the resistivity of Sr_2RuO_4 with temperature between T_c and 300 K is shown in Fig. 3. The resistivity along the ab planes is metallic ($d\rho_{ab}/dT > 0$) and shows superlinear dependence on T over the measured temperatures with a large residual resistivity ratio $\rho_{ab}(300\ \mathrm{K})/\rho_{ab}(1\ \mathrm{K}) \sim 150$ and with a very small residual resistivity of $\rho_{ab} \sim 1\ \mu\Omega$cm just above T_c. In contrast, the resistivity along the c axis is non-metallic with negative $d\rho_c/dT$ at temperatures above $T_M \sim 130$ K, but becomes metallic at temperatures below T_M. Therefore, there is a crossover at T_M from the two dimensional to the three dimensional metal with decreasing temperature. The square of the anisotropy ratio estimated from the resistivities just above T_c is $\Gamma_N^2 = m^*_c/m^*_{ab} = \rho_c/\rho_{ab} \approx 400$, where m^*_{ab} and m^*_c are the effective masses of the quasiparticles for the motion in the ab planes and along the c axis, respectively [21]. This large anisotropy, reflecting its layered structure, agrees well with the ratio of the Fermi velocities estimated from the Fermi-surface parameters obtained from the quantum oscillations [5]. It should be noted that the resistivities along both the ab planes and the c axis below about 25 K follow the T-squared dependence quite precisely: $\rho = \rho_0 + AT^2$, as shown in Fig. 4. By fitting the ρ-T curves, we obtained $A_{ab} = 7.3\ \mathrm{n\Omega cm/K^2}$ and $A_c = 4.0\ \mu\Omega\mathrm{cm/K^2}$. This T-squared dependence implies the importance of the Umklapp process of the electron-electron scattering at low temperatures, consistent with the formation of the Fermi liquid state.

3.1.2 Susceptibility

The variation of the magnetic susceptibility with temperature under a field H of 1 T is shown in Fig. 5. In contrast with the large anisotropy of the resistivity, the magnetic susceptibility depends only weakly on the direction of the external field: $\chi_{ab} = 0.88 \times 10^{-3}$ emu/mol (H // ab) and $\chi_c = 0.98 \times 10^{-3}$ emu/mol (H // c) at 300 K, respectively, after correction for the isotropic core diamagnetism of $\chi_{core} = -0.96 \times 10^{-4}$ emu/mol [22]. These values of χ_{ab} and χ_c are enhanced by a factor of ~ 4 from that observed in the ordinary d-band metal RuO_2, for which the susceptibility is 0.2×10^{-3} emu/mol at 300 K after the diamagnetic correction of -0.42×10^{-4} emu/mol [22]. The gradual increase of χ_{ab} and χ_c below about 200 K might be attributable to small inclusions (≤ 0.04 %) of ferromagnetic $SrRuO_3$ (T_{Curie} ~ 160 K). Both χ_{ab} and χ_c exhibit weak temperature dependence up to 700 K with a weak and broad maximum at about 500 K. This maximum is often observed in the weakly anisotropic quadratic-layer antiferromagnet [21]. The large magnitudes and the small temperature dependence of χ_{ab} and χ_c, however, cannot be solely fitted with those expected for the two-dimensional Heisenberg model with $S = 1$ [23].

From the argument above, we deduce that the large and weakly T-dependent χ_{ab} and χ_c consist of the temperature-independent paramagnetic contributions: $\chi_i = \chi_0 + \chi_{VV,i}$ ($i = ab$ or c). Here, χ_i is the susceptibility after correction for the core diamagnetism, χ_0 is the isotropic Pauli spin paramagnetic susceptibility and $\chi_{VV,i}$ is the anisotropic Van Vleck susceptibility. It is generally difficult to estimate the magnitude of the Van Vleck susceptibility. We note that for the corresponding cuprate $La_{2-x}Sr_xCuO_4$, a band-structure prediction of $\chi_{VV} = 0.15 \times 10^{-4}$ emu/mol (H // ab) and 0.4×10^{-4} emu/mol (H // c) for Sc_2CuO_4 [24] is often used. Considering the difference in the symmetry of the relevant d orbitals of the ruthenates and the cuprates, the anisotropy of $\chi_{VV,i}$ would be sufficient to explain the difference between χ_{ab} and χ_c of Sr_2RuO_4. In other words, the anisotropy in Sr_2RuO_4 is probably attributed to the small and anisotropic contribution of χ_{VV} to χ. From the above consideration, χ_{ab} and χ_c are most likely dominated by an enhanced Pauli spin susceptibility χ_0, and in the remainder of the paper we conveniently make the approximation that $\chi_0 \approx \chi_{ab}$ or χ_c.

3.1.3 Specific heat

Figure 6 shows the specific heat divided by temperature C_P/T above 2 K for zero field and under a magnetic field of 14 T applied parallel to the c axis [25]. Fitting with $C_P/T = \gamma + \beta T^2$ gives the Sommerfeld constant of $\gamma = 37.5$ mJ/K^{2}mol and $\beta = 0.191$ mJ/K^{4}mol for zero field. The

Debye temperature Θ_D is estimated as ~ 410 K using the relation $\Theta_D = (12\pi^4 N k_B/5\beta)^{1/3}$, where N is the number of atoms per mol and k_B is the Boltzmann constant. The density of states at the Fermi level estimated from γ is enhanced from the theoretical expectation based on the band-structure calculation by a factor of 3.6. A similar enhanced γ has also been observed in recent investigations using polycrystalline samples [26]. This enhancement is too large to be account for solely by the electron-phonon interaction. It should be noted that even with the field of 14 T, γ does not change within our experimental accuracy of ± 1.5 mJ/K^{2}mol. This indicates that the enhancement does not originate from weak spin fluctuations. In fact, recent photoemission measurements [7] suggest the presence of the coherence peak at the Fermi level, expected in a strongly correlated system in the vicinity of a Mott-Hubbard insulator. The band width of the coherent states is estimated as ~ 0.3 eV, corresponding the magnetic energy of 5000 T. Therefore, we conclude that the enhanced γ is attributed to the increased density of states by the strong electronic correlation.

3.2 Highly anisotropic Fermi liquid state

Let us discuss whether the strong electronic correlations in the normal state of Sr_2RuO_4 is related to the appearance of the Fermi liquid state. One of the parameters to characterize the Fermi-liquid state, frequently used for heavy-Fermion materials, is the Wilson ratio, $R_W \equiv (\pi^2 k_B^2/3\mu_B^2)(\chi_0/\gamma)$, where μ_B is Bohr magneton, χ_0 is the Pauli spin susceptibility expressed in emu/mol, and γ is expressed in erg/K^{2}mol (= 10^{-4} mJ/K^{2}mol). R_W is unity for a free electron gas, and is expected to increase up to two if the enhancements of both χ_0 and γ are attributable to the same origin of the strong correlations among electrons [27]. On the other hand, $R_W \gg 1$ if χ_0 is mainly enhanced by ferromagnetic spin correlations, and $R_W < 1$ if γ is mainly enhanced by strong electron-phonon correlations.

In Fig. 7 we plot χ_0 against γ for Sr_2RuO_4 along with many highly correlated electron systems including heavy-Fermion compounds. R_W = 1.7 - 1.9 for Sr_2RuO_4 is comparable to that of compounds with the Fermi-liquid state and suggests the strong electronic correlation as a common origin of the enhancements in the susceptibility and the electronic specific heat.

Secondly, we examine the Kadowaki-Woods ratio [28] which is defined as the ratio A/γ^2, where A is the coefficient of the T^2 term of the resistivity. Phenomenologically it is expected to take the universal value $a_0 = 1.0 \times 10^{-5}$ μΩcm/(mJ/Kmol)^2 as long as the conduction and the enhanced γ are governed by the same quasiparticles with a self-energy that depends strongly on

frequency [29]. It is also known that for systems without such mass renormalization, A/γ^2 is consistently smaller than a_0 by a factor of about 25.

In Fig. 8 we plot A against γ for Sr_2RuO_4 along with many highly correlated electron systems including heavy-Fermion compounds, as well as some transition metals. The ratio for the in-plane conduction $A_{ab}/\gamma^2 = 0.52a_0$ is in fair agreement with the universal trend. This confirms that the same quasiparticle states probed by the enhanced electronic specific heat predominate the conduction within the RuO_2 planes. This consideration is strongly supported by the fact that the obtained γ is well comparable to $\gamma = 32$ mJ/K^{2}mol estimated from the cyclotron masses of the quasiparticles for the motion in the *ab* planes determined by the quantum oscillations [5] using the following relation:

$$\gamma = (1/3)\pi^2 k_B^2 D(\varepsilon_F) N_A = 1.47 \Sigma m^*_{ab}/m_e \ \text{mJ/K}^2\text{mol}, \qquad (3.1)$$

where $D(\varepsilon_F) = (a^2/\pi\hbar^2)m^*_{ab}$ is the electronic density of states of a two dimensional system, N_A is the Avogadro's number, m_e is the bare electron mass, and the summation is taken over all the Fermi-surface components. In contrast, $A_c/\gamma^2 = 280a_0$ severely deviates from the universality. This ratio originates from the interlayer conduction which is characterized by a small velocity component v_c of the same quasiparticles; v_c is associated with the slight dispersion along the c axis of the nearly cylindrical Fermi surface. In this sense, the observed A_c reflects the renormalized effective mass of the quasiparticles for the motion along the c axis given by $m^*_c = m^*_{ab}(v_{ab}/v_c)^2/2$. This ratio $(v_{ab}/v_c)^2/2$ is expected to be greater than 550, if it is estimated from the Fermi surface parameters inferred from the quantum oscillations [5]:

$$(v_{ab}/v_c)^2/2 = (4/c^2)\{\Sigma(k_F^2/m^*_{ab})_i / \Sigma(k_F^2 \Delta k_F^2/m^*_{ab})_i\}, \qquad (3.2)$$

as described in the next section. This value is in good agreement with the observed $A_c/A_{ab} \approx 550$. From the above considerations, we conclude that the normal state of Sr_2RuO_4 is described as a highly anisotropic Fermi-liquid state.

3.3 Anomalous temperature dependence of resistivity along the *c* axis

As mentioned in Sec. 3.1.1, the resistivity along the c axis of Sr_2RuO_4 exhibits curious temperature dependence: the crossover from the metallic to non-metallic behavior at $T_M \sim 130$ K with increasing temperature. It is well known that ρ_c of $La_{2-x}Sr_xCuO_4$ is profoundly affected by the structural transition from the high-temperature tetragonal phase to the mid-temperature orthorhombic phase [11]. Our investigation of powder X-ray diffraction at low temperatures [2, 30] shows that Sr_2RuO_4 does not exhibit any structural transition down to 5 K or any change in

the temperature dependence of the lattice parameters across T_M. This result is consistent with recent electron diffraction [31], Raman-scattering [32] and neutron-scattering [33] measurements. Therefore, the origin of the sign change in $d\rho_c/dT$ with temperature in the present system appears to be purely electronic. Since the mechanism of the dimensional crossover in the metallic conduction is an important issue in HTSC, it is of great interest to understand the crossover mechanism in Sr_2RuO_4.

Let us discuss what criteria determine the boundary between the metallic and nonmetallic conduction at $T = T_M$, as well as that between the Fermi-liquid behavior and non-Fermi-liquid behavior at $T \approx 25$ K. We will analyze the temperature dependence of ρ_c from the viewpoint of the relaxation time, or the life time, for scattering of the quasiparticles. (The derivation in this section is motivated by the argument in Ref. 5, which adopted the approximation of a common mean-free-path.)

First, we consider the criterion for the Fermi-liquid description. The resistivity along the c axis ρ_c of Sr_2RuO_4 is associated with a small velocity component of the quasiparticles, as discussed in Sec. 3.2. Let us define the characteristic time for the quasiparticles to move between adjacent RuO_2 planes as τ_c (= d/v_c), where $d = c/2$ is the interlayer spacing and v_c is the rms group velocity along the c direction of the Fermi surface. When the life time τ of the quasiparticles is shorter than τ_c, the coherent metallic conduction in that direction is not expected to occur.

We consider an energy dispersion for each band near the Fermi level of the elementary form

$$\delta \varepsilon_k = \hbar^2 k_F \delta k_F / m^*_{ab} - 2t_c \cos(k_c c), \tag{3.3}$$

where t_c and k_c represent a hopping matrix element and the wavevector, respectively, and $\hbar = h/2\pi$ as h is the Plank constant. This results in the relations

$$v_c = \sqrt{2}\, t_c c/\hbar \quad \text{and} \quad t_c = \hbar^2 k_F \Delta k_F/(4m^*_{ab}), \tag{3.4}$$

where Δk_F is the dispersion along the c axis for each Fermi surface. Using these relations we obtain the rate at which the quasiparticles travel to the adjacent planes as

$$1/\tau_c = 2\sqrt{2}\, t_c/\hbar = \hbar k_F \Delta k_F/(\sqrt{2}\, m^*_{ab}). \tag{3.5}$$

From the Fermi-surface parameters determined from the quantum oscillations [5], we can estimate the characteristic transfer rate $1/\tau_c$ for each Fermi surface as summarized in Table 1:

$$1/\tau_c = 4.5 \times 10^{11}\ \text{s}^{-1} \text{ for the } \alpha\text{-Fermi surface},$$
$$= 6.3 \times 10^{12}\ \text{s}^{-1} \text{ for the } \beta\text{-Fermi surface},$$
$$= 3.4 \times 10^{12}\ \text{s}^{-1} \text{ for the } \gamma\text{-Fermi surface}.$$

We note that the transfer rate is greatest for the β-Fermi surface, and is larger by an order of

magnitude than that for the α-Fermi surface.

Let us estimate the life time τ at low temperatures, which is governed by the relaxation time of the impurity scattering τ_{imp} and that of the electron-electron scattering τ_{ee}. We use the Drude relationship $\sigma = \Sigma\ (ne^2\tau/m^*)_i$, where σ is the conductivity, n is the carrier number, e is the elementary electronic charge, m^* is the effective mass of the quasiparticles and Σ_i represents the summation over the Fermi-surface branches designated by i (parallel resistivity for different bands). Using the relation $n_i = k_{F,i}^2/\pi c$ (for the two-dimensional system) and $m^*_{c,i} = m^*_{ab,i}(v_{ab,i}/v_{c,i})^2/2$,

$$\sigma_{ab} = \Sigma\ (ne^2\tau/m^*_{ab})_i = (e^2/\pi c)\Sigma(k_F^2\tau/m^*_{ab})_i, \quad (3.6a)$$

$$\sigma_c = \Sigma\ (ne^2\tau'/m^*_c)_i = (e^2c/4\pi)\Sigma(k_F^2\Delta k_F^2\tau'/m^*_{ab})_i. \quad (3.6b)$$

In these equations, we omit the index i for the quantities within the summation for brevity. We can set $\tau' = \tau$ for each band because the conductivities are governed by the life time of common quasiparticles. In fact, the expected anisotropy ratio of the resistivity $\rho_c/\rho_{ab} = \sigma_{ab}/\sigma_c = (4/c^2)\{\Sigma(k_F^2/m^*_{ab})_i/\ \Sigma(k_F^2\Delta k_F^2/m^*_{ab})_i\} \approx 550$ is consistent with our observation.

At high temperatures, it is a good approximation that the life time is limited by the thermal process and is therefore independent of the location on the Fermi surfaces (the common-τ approximation). On the other hand, at lowest temperatures, it is a good approximation that the mean free path along the ab planes l_{ab} is independent of the Fermi surfaces because it is in the impurity scattering limit;

$$l_{ab} = v_{ab,i}\tau_i = \hbar k_{F,i}\tau_i/m^*_{ab,i} = \text{constant and common to } \alpha,\ \beta \text{ and } \gamma. \quad (3.7)$$

Since $k_{F,i}/m^*_{ab,i}$ estimated from the Fermi surface parameters of Sr_2RuO_4 (Table. 1) fortunately does not depend much on the band, the common-l_{ab} approximation is crudely equivalent to the common-τ approximation according to eq. (3.7). Therefore, we adopt the common-τ approximation for all temperature range, which would retain semi-quantitative validity.

In this common-τ approximation, we will express ρ_{ab} in order to evaluate the transfer rate for the electron-electron scattering $1/\tau_{ee}$ and for the impurity scattering $1/\tau_{imp}$. We consider the series resistivity for different scattering: $1/\sigma_i = \Sigma_j(1/\sigma_{ij})$, where Σ_j represents the summation over scattering processes of the quasiparticles designated by j (j = ee for the quasiparticle scattering and j = imp for the impurity scattering). Along with eq. (3.6a), we obtain

$$1/\sigma_{ab,i} = \Sigma_j(1/\sigma_{ab,ij}) = (\pi c/e^2)(m^*_{ab,i}/k_{F,i}^2)\Sigma_j(1/\tau_j). \quad (3.8)$$

Moreover, from the parallel resistivity for different bands: $\rho_{ab} = \{\Sigma_i(\sigma_{ab,i})\}^{-1}$, we obtain

$$\rho_{ab} = \frac{\pi c}{e^2}\left(\sum_i \frac{k_{F,i}^2}{m^*_{ab,i}}\right)^{-1}\sum_j \frac{1}{\tau_j} \qquad (3.9)$$

Note that the first summation in eq. (3.9) can be fully evaluated using the Fermi-surface parameters given in Table 1.

From $\rho_{ab} = \rho_{ab,0} + A_{ab}T^2$, we evaluate the transfer rate for the electron-electron scattering $1/\tau_{ee}$ and for impurity scattering $1/\tau_{imp}$ as

$$1/\tau_{imp} = (e^2\rho_{ab,0}/\pi c)\Sigma_i(k_{F,i}^2/m^*_{ab,i}) \qquad (3.10a)$$

$$= 8.2 \times 10^{11}\ s^{-1} = \text{constant and common to } \alpha, \beta \text{ and } \gamma.$$

$$1/\tau_{ee} = (e^2A_{ab}T^2/\pi c)\Sigma_i(k_{F,i}^2/m^*_{ab,i}). \qquad (3.10b)$$

Figure 9 shows the variations of $1/\tau_c$, $1/\tau_{ee}$ and $1/\tau_{imp}$ with temperature. For the band α, $1/\tau$ ($=1/\tau_{ee} + 1/\tau_{imp}$) is larger than $1/\tau_c$ even at $T = 0$ K. On the other hand, for β, $1/\tau$ is less than $1/\tau_c$ below about 25 K. Therefore, the coherent metallic conductivity along the c axis should be maintained below 25 K. This explains why the T-squared dependence of ρ_c is observed below 25 K, despite the large magnitude of ρ_c of a few mΩcm and the nearly two-dimensional character of the Fermi surfaces.

Second, we discuss the criterion for the metal–non-metal crossover of ρ_c by comparing the relaxation time τ_{ep} of the quasiparticles scattered by phonons and τ_c. The transfer rate for the electron-phonon scattering $1/\tau_{ep}$ is proportional to k_BT;

$$1/\tau_{ep} = Ck_BT/\hbar, \qquad (3.11)$$

where C is the dimensionless proportional coefficient. Between 25 K and 130 K, where the coherent metallic description breaks down, the resistivity along the c axis is nevertheless metallic with $d\rho_c/dT > 0$. This is probably attributed to finite probability that the quasiparticles travel without scattering by phonons, which predicts $\rho_c \propto \rho_{ab}$ [34].

On the other hand, when the thermal energy is larger than the effective band width W, the velocity distribution of the quasiparticles is too heavily disturbed to maintain the Drude description for metallic conduction. In the tight-binding model, W is $2zt$, where z is the numbers of the nearest neighbor atomic sites and t is the hopping matrix. We use $W = 4t_c$ ($z = 2$) for the conduction along the c axis in Sr_2RuO_4. Using this relation and equations (3.4) and (3.5), we can express the rate at which the quasiparticles travel to the adjacent planes as

$$1/\tau_c = W/(\hbar\sqrt{2}). \qquad (3.12)$$

When $1/\tau_{ep}$ is larger than $1/\tau_c$, it is expected that the metallic conduction in the Drude description changes to the non-metallic conduction by the thermally assisted hopping. We believe that this is the crossover that occurs at T_M. From the fact that $1/\tau_c$ for the β-Fermi surface is the largest among the three bands, we determine the coefficient C in (3.12) by assuming that the crossover for the β-Fermi surface gives T_M for the boundary of the metal-non metal, as shown in Fig. 9:

$$C = W^*/k_B T_M, \tag{3.13a}$$

$$\text{with} \quad W^* = W/\sqrt{2}, \tag{3.13b}$$

where W^* is defined as the effective band width. This analysis gives $W^* = 2\sqrt{2}\,t_c$. Therefore, we estimate $C = 0.37$ using $t_c = 17$ K for the β-Fermi surface. In addition, when we use the obtained $1/\tau_{ep}$ for the other band based on the common-τ approximation, the transfer rate for the electron-phonon scattering predicts similar crossover of ρ_c at ~ 70 K for γ-Fermi surface, as shown in Fig. 9. This coincides with the temperature of 65 K above which ρ_c deviates downward from the relation $\rho_c \propto \rho_{ab}$, as shown in Fig. 10.

Next we discuss the temperature dependence of ρ_{ab}. With increasing temperature, it starts to deviate from the T^2-dependence at 25 K, as well as ρ_c. The time τ_a for the quasiparticles to move between the nearest Ru atoms is represented by

$$1/\tau_a = v_{ab}/a. \tag{3.14}$$

Here, a is the lattice parameter along the a axis. The estimated $1/\tau_a$ using the Fermi-surface parameters is larger by two orders of magnitude than the relaxation time $1/\tau$ ($=1/\tau_{ee} + 1/\tau_{imp}$) at 25 K. Therefore, the coherent conduction along the ab planes should not be disturbed at this temperature. In this sense, it is of great interest why the Fermi-liquid description breaks down for ρ_{ab} above 25 K. In addition, at 65 K and 130 K, the temperature dependence of ρ_{ab} qualitatively changes: $\rho_{ab} - \rho_{ab,0} \propto T^{1.55}$ (25 K ≤ T ≤ 65 K), $T^{1.37}$ (65 K ≤ T ≤ 130 K) and $T^{1.50}$ (130 K ≤ T), as shown in Fig. 11. Clarification of the relationship between ρ_{ab} and ρ_c is quite important for the understanding of the electronic states in Sr_2RuO_4.

In order to confirm the above considerations, it is very useful to study the Fermi-liquid behavior by means of impurity doping in the RuO_2 planes. Such impurities can control the life time of the quasiparticles, and as a consequence the effective dimensionality of the conduction. In addition, it is also desirable to study the crossover between the metallic and non-metallic conduction by measurements under pressures, which controls the hopping matrix element t_c.

4. Superconducting Properties

In this chapter, we first show that Sr_2RuO_4 is a highly anisotropic 3D superconductor based on the superconducting parameters determined from T_c and the upper critical fields H_{c2} [35]. Secondly, we will show that the peculiar flux dynamics found is originated from the anisotropy of the superconductivity [36].

4.1 Anisotropic superconducting state

4.1.1 Anisotropic upper critical fields H_{c2}

Figure 12 shows the variations of the real part of ac susceptibility χ' with H_{dc} at selected temperatures for an ac field H_{ac} = 0.58 Oe, parallel to H_{dc}, at a frequency of f = 1000 Hz. With increasing temperature, the onset of diamagnetic susceptibility shifts to lower field and is not observed above 1 K. In this study $H_{c2}(T)$ is defined as the intersection of the linear extrapolation of the most rapidly changing part of χ' with that of normal-state χ', as indicated in Fig. 12. Although this definition will somewhat underestimate the true H_{c2}, we adopted this definition here for convenience. It should be noted that $H_{c2//ab}(T)$ is an order of magnitude larger than $H_{c2//c}(T)$. It is interesting that a peak structure in χ' appears below H_{c2} only when $H_{dc}(//H_{ac})$ is parallel to the *ab* planes. We will discuss this peak structure in detail in the next section. In this section, we concentrate on the anisotropic H_{c2}.

Shown in Fig. 13 is the H-T phase diagram obtained from the χ'-H curves, which is consistent with that derived from χ'-T curves. T_c defined as $T(H_{c2})$ in the limit of $\mu_0 H_{dc} = 0$ T is 0.90 K. Extrapolation of H_{c2}-T curves to 0 K gives $\mu_0 H_{c2//ab}(0) = 0.78$ T and $\mu_0 H_{c2//c}(0) = 0.030$ T. These values are smaller than the Pauli limiting field

$$\mu_0 H_{Pauli} = 1.24 k_B T_c/\mu_B = 1.66 \text{ T} \qquad (4.1)$$

simply expected from the BCS theoretical calculation [37]; the small H_{c2} values mean that the pair breaking effects due to the Zeeman energy are negligible. Here, k_B is the Boltzmann constant and μ_B is the Bohr magneton. These $H_{c2}(0)$ are in good agreement with those derived from the Werthamer-Helfand-Hohenberg formula [38],

$$H_{c2}(0) = 0.693(dH_{c2}/dT)_{Tc} T_c, \qquad (4.2)$$

obtained for the weak-coupling BCS theory. The electron-phonon coupling constant $\lambda_{e\text{-}p} = 0.37$, estimated on trial from the McMillan formula [39] using T_c = 0.90 K, the Debye temperature Θ_D = 410 K and the Coulomb repulsion parameter μ^* = 0.10, implies that Sr_2RuO_4 is not in the strong coupling regime; both T_c and Θ_D are similar to those of aluminum. The anisotropy in the coherence lengths, $\Gamma_S = \xi_{ab}(0)/\xi_c(0) = 26$, agrees well with the square root of the effective mass

ratio Γ_N in the normal state of this anisotropic Fermi liquid. Therefore, the superconductivity in Sr_2RuO_4 originates from Cooper pairs formed by the highly correlated electrons. In this respect, although we do not have any information yet to specify the symmetry of the Cooper pairs, the possibility of unconventional superconductivity cannot be excluded.

4.1.2 Anisotropic superconducting parameters

Using the Ginzburg-Landau (G-L) formula for an anisotropic 3D superconductor,

$$H_{c2//c} = \phi_0/(2\pi\,\xi_{GLab}^2) \text{ and } H_{c2//ab} = \phi_0/(2\pi\,\xi_{GLab}\,\xi_{GLc}), \tag{4.3}$$

where ϕ_0 is the flux quantum, we estimated the coherence lengths of $\xi_{GLab}(0) = 1.05\times10^3$ Å and $\xi_{GLc}(0) = 40$ Å. Moreover, using

$$\xi_0 = \alpha\,\hbar v_F/k_B T_c, \tag{4.4}$$

where $\alpha = 0.18$ for the BCS theory, $\hbar = h/2\pi$ as h is the Plank constant and v_F is the Fermi velocity, we obtained $v_{ab} = 6.9\times10^4$ m/s and $v_c = 2.6\times10^3$ m/s for v_F estimated from $\xi_{GLab}(0)$ and $\xi_{GLc}(0)$, respectively. These values are consistent with those obtained from the quantum oscillation experiment in the normal state [5], but substantially smaller than those from a band calculation [4]. A large value for the superconducting anisotropy $\xi_{GLab}(0)/\xi_{GLc}(0) = 26$ is compared with ~ 10 of $La_{1.86}Sr_{0.14}CuO_4$ [40].

There is an important difference between Sr_2RuO_4 and HTSC as ξ_{GLc} is compared with the interlayer distance d. For Sr_2RuO_4, ξ_{GLc} is larger than the interlayer spacing $d = c/2 = 6.37$ Å by a factor of 6, in contrast to $\xi_{GLc} \le 3$ Å $< d$ for $La_{1.86}Sr_{0.14}CuO_4$ [40]. In this sense, Sr_2RuO_4 is an extremely anisotropic, but 3D superconductor.

Now various superconducting parameters can be estimated using relevant theoretical relations. The BCS relation

$$H_c(0)^2 = \gamma T_c^2/0.17, \tag{4.5}$$

where $\gamma = 6.53\times10^3$ erg/K^2 cm^3 (= 37.5 mJ/K^2 mol), gives the thermodynamic critical field $\mu_0 H_{c0} = 0.018$ T. The anisotropic G-L parameters are evaluated from

$$H_{c2}(0) = \sqrt{2}\,\kappa(0) H_c(0) \tag{4.6}$$

to be $\kappa_{ab}(0) = 31$ and $\kappa_c(0) = 1.2$. Therefore, Sr_2RuO_4 is a type II superconductor with nearly a type- I character for the length scales within the ab planes. From

$$\kappa_c = \lambda_{ab}/\xi_{GLab} \text{ and } \kappa_{ab} = (\lambda_{ab}\lambda_c/\xi_{GLab}\,\xi_{GLc})^{1/2}, \tag{4.7}$$

estimations for the penetration depths are $\lambda_{ab}(0) = 1.3\times10^3$ Å and $\lambda_c(0) = 3.3\times10^4$ Å. Using

$$H_{c1}(0)H_{c2}(0) = H_c(0)^2(\ln\kappa(0) + 0.08) \text{ valid for } \kappa \gg 1 \tag{4.8a}$$

$$H_{c1}(0)H_{c2}(0) \approx H_c(0)^2 \text{ valid for } \kappa \approx 1, \quad (4.8b)$$

the lower critical fields are $\mu_0 H_{c1}(0) = 1.4$ mT (//*ab*) and 0.011 T (//*c*). The mean-free-paths from ref. [5], $l_{ab} \sim 1.0\times10^3$ Å and $l_c \sim 30$ Å (see also section 3-3), are almost the same as the coherence lengths; this indicates that Sr_2RuO_4 is not in the clean limit, in contrast with HTSC. All the parameters of anisotropic superconductivity thus evaluated are summarized in Table 2.

4.2 Peculiar flux pinning in the mixed state

4.2.1 Detailed experimental procedure

In order to investigate the mechanism of the peculiar anisotropic peak structure of Sr_2RuO_4, as described above, we measured ac susceptibility (χ', χ'') under magnetic fields $\mu_0 H_{dc}$ up to 8 T with a variety of configurations between H_{dc} and H_{ac} . Here, H_{dc} and H_{ac} are applied either along the *ab* planes or along the *c* axis; there are five distinct configurations of the directions of H_{dc} and H_{ac} with respect to the crystalline axes, as shown in Fig. 14. Figure 14 (a) and (b) depict the longitudinal configurations with H_{dc} // H_{ac}, which provide compressional motions of flux lines. These are the same configurations used for the investigation of the anisotropic H_{c2}. The others, Fig. 14 (c)-(e) show the transverse configurations with $H_{dc} \perp H_{ac}$, which provide the tilting motions of flux lines. It is difficult in our present experimental setup to exactly align H_{dc}, H_{ac} and crystalline axes. Because of large anisotropy in $H_{c2}(0)$, 0.78 T for H_{dc} // *ab* and 0.030 T for H_{dc} // *c*, H_{c2} is quite sensitive to the orientation of H_{dc} with the *ab* planes. Assuming that H_{c2} varies with the angle θ between H_{dc} and the *ab* planes as

$$H_{c2}(\theta) = H_{c2//ab}\{\cos^2\theta+(H_{c2//ab}/H_{c2//c})^2\sin^2\theta\}^{-1/2} \text{ [41]}, \quad (4.9)$$

we can estimate the misalignment angle in this study to be less than 1.5 °. In order to minimize the influence of the magnetization relaxation during the field sweep, we employed a very slow sweep rate of H_{dc}, 0.5 T/hr (H_{dc} // *ab*) and 0.05 T/hr (H_{dc} // *c*). The results with the slow field sweep agree with those with a field held constant for each measurement. Moreover, the field-sweep results gave the consistent phase boundary as *T*-sweep results. These confirm that the influence of the magnetization relaxation is not important in describing the present results.

4.2.2 Peak effect with dc field along the *ab* planes

The results for the longitudinal configurations are represented in Fig. 15, showing the variations of the real and imaginary components of ac susceptibility (χ', χ'') with H_{dc} at $T \ll T_c$. It is interesting to note that a peak structure in χ' appears below H_{c2} only when $H_{dc}(//H_{ac})$ is

parallel to the *ab* planes, as described above. The corresponding second dissipation peak is also observed in the χ''-H curve below the ordinary pronounced peak near $H_{c2}(T)$, as shown in the upper part of Fig. 15 (a). With increasing H_{dc}, χ'' first increases linearly, which implies that χ'' is proportional to the number of vortices, and then takes a maximum, the field of which we define as $H_p(T)$. This maximum indicates that the number of the flux lines trapped in pinning centers increases rapidly just above $H_p(T)$. The crystals used in this study have a single sharp peak in the χ''-T curve with $H_{dc} = 0$ T, indicating high homogeneity of the transition temperature throughout the crystal. Moreover, essentially the same second peak is observed also in the crystals with different ΔT_c. Therefore, the second peak is not attributable to the coexistence of the phases with different T_c, but must be intrinsic to the superconductivity of Sr_2RuO_4. The field-sweep results presented here are taken with increasing fields after zero-field cooling (ZFC). Actually we measured susceptibility with both increasing and decreasing H_{dc} and observed a minor quantitative but no qualitative difference between the two procedures. The difference can be ascribed almost entirely to a technical artifact due to the time constant, $\tau \sim 20$ s, of the magnet used. In addition, the difference between the results under ZFC and field cooling is negligible.

The variations of χ' and χ'' with H_{dc} in the transverse configurations ($H_{dc} \perp H_{ac}$) at about 0.4 K are shown in Fig. 16. The second peak similar to the one in the longitudinal configuration (Fig. 15 (a)) is also observed for (H_{dc} // *ab*) $\perp$ (H_{ac} // *ab*) (Fig. 16 (a)). However, χ'' tends to saturate before reaching the peak, in contrast with the linear increase up to the peak for (H_{dc} // *ab*) // (H_{ac} // *ab*). This is possibly due to the misalignment. In fact, the obtained $H_{c2}(T)$ is a little smaller than the $H_{c2}(T)$ for (H_{dc} // *ab*) // (H_{ac} // *ab*). This difference can be explained by a misalignment of $\Delta\theta \sim 1.5$ °, estimated by the angle-dependent $H_{c2}(\theta)$ given by the equation (4.9). These observations indicate also that the second-peak phenomenon reported here is not too sensitive to the exact alignment of H_{dc} with the *ab* planes.

When the flux lines within the *ab* planes (H_{dc} // *ab*) are tilted towards the *c* axis (H_{ac} // *c*), the dissipation at low fields is substantially reduced and the second peak is barely visible (Fig. 16 (b)). For (H_{dc} // *c*) $\perp$ (H_{ac} // *ab*) (Fig. 16 (c)), we observed only the peak corresponding to H_{c2} at all temperatures below T_c, similar to the longitudinal observation with H_{ac} // *c* and H_{dc} // *c*.

4.2.3 Field and temperature dependence of H_p

In order to further characterize the peak effect, we will concentrate on the longitudinal configuration with (H_{dc} // *ab*) // (H_{ac} // *ab*), for which the effect was most clearly observed. The

variations of χ' with H_{dc} at selected temperatures are previously plotted in Fig. 12 (a). The second peak structure is not observed above 0.77 K. The corresponding variations of χ'' with H_{dc} are shown in Fig. 17 (a). With increasing H_{dc}, the dissipation at all temperatures first increases along a common line up to the second peak. As a result, the second peak height, χ'' at $H_p(T)$, varies linearly with $H_p(T)$. This is in sharp contrast with the relation between the first peak height and H_{c2}: the height of this peak decreases with increasing $H_{c2}(T)$ as shown in Fig. 17 (b).

The obtained $H_p(T)$ is plotted in Fig. 18 along with the upper critical fields $H_{c2//ab}(T)$ and $H_{c2//c}(T)$. With increasing temperature, $H_p(T)$ decreases from $H_p(0) \approx 0.45$ T, estimated by the extrapolation of the H_p-T curve to 0 K, and vanishes continuously at about $0.8T_c$. The $H_p(T)$ clearly does not merge into $H_{c2}(T)$ even at T_c.

Figure 19 shows the variations of longitudinal χ' and χ'' with temperature at selected H_{dc} parallel to the ab planes. For $H_{dc} < H_p(0)$, χ'' initially remains constant with increasing temperature (Fig. 19 (a)). This behavior strongly supports the above interpretation that the dissipation below $H_p(T)$ depends linearly on the number of vortices, because the number remains essentially constant during this T-sweep. Further increasing T results in a small dip in χ'', which is accompanied by the decrease in χ' indicating the recovery of pinning force. On the other hand, the T-sweep measurements with constant fields at $0.5 \text{ T} \leq \mu_0 H_{dc} \leq 0.7$ T show that χ' and χ'' decrease from the lowest temperatures (Fig. 19 (b)). This behavior is understandable because for $H_{dc} > H_p$ a T-sweep process never crosses the $H_p(T)$ line. While there is no obvious second peak in the χ''-T curves even for $H_{dc} < H_p$, the onset temperature of the decreasing χ'' at each H_{dc} well corresponds to $T(H_p)$, as plotted by open squares in Fig. 18.

4.2.4 Frequency independence of H_p

We investigated the effect of the frequency f of H_{ac} on the χ'-T and χ''-T curves at $\mu_0 H_{dc} = 0.50$ T. Because $T(H_p)$ is not defined in this region of $H_{dc} > H_p(0)$, the temperature at which χ'-T curve takes the minimum is denoted as $T(H_p')$, in which H_p' is defined as the corresponding minimum field in the χ'-H curve, as indicated in Fig. 19 (b). This H_p' corresponds to the changeover field from the increasing flux-pinning near H_p to flux-depinning near H_{c2}. The temperature dependence of H_p' corresponds qualitatively well to that of H_p, as shown in Fig. 20. Therefore, $T(H_p')$ is also the characteristic temperature of the peak effect. We show the variation of $T(H_p')$ with the frequency in Fig. 21. $T(H_p')$ is nearly independent of the frequency of H_{ac}

between 10^2 and 10^4 Hz. In contrast, $T(H_{c2//ab})$ varies as

$$f = f_0 \exp(-U_0/k_B T), \tag{4.10}$$

where U_0 = 0.7 meV is the estimated pinning potential and k_B is the Boltzmann constant. Therefore the first dissipation peak near H_{c2} can be explained in terms of thermally activated flux motions, whereas a different process is required to explain the second dissipation peak.

4.2.5 Peculiar anisotropic flux pinning

The second dissipation peak in the χ''-H curve indicates a recovery of the flux pinning force. As we have shown, the second peak is observed only with H_{dc} // ab. Moreover, it is most prominent for H_{ac} // ab, while it is much suppressed and barely visible for H_{ac} // c. As long as both H_{dc} and H_{ac} are within the ab planes, the second peak is clearly observed regardless of the configuration between H_{dc} and H_{ac} . In HTSC, in contrast, the peak effects have often been reported for H_{dc} // c. They are attributable to the melting transition from the vortex solid to the vortex liquid with mainly increasing temperature [42], or in other cases to the crossover from the 3D to 2D pancake vortices with increasing field [43]. A conventional 3D superconductor with a layered structure, 2H-$NbSe_2$ with T_c = 7.6 K and the anisotropy parameter Γ_S = 3.3, exhibits a peak effect for both H_{dc} // ab [44] and H_{dc} // c [45], interpreted as a crossover of the vortex dynamics from the coherent motion to a plastic flow with increasing field. In κ-(BEDT-TTF)$_2$Cu[N(CN)$_2$]Br with the highest T_c of 10.9 K known among the organic superconductors and with Γ_S = 4 [46], the peak effect is absent at least in the ac susceptibility for H_{dc} // c [47]. A crucial difference in the superconductivity of Sr_2RuO_4 in comparison with that of HTSC is that the coherence length $\xi_c(0)$ = 40 Å, which is larger than the interlayer spacing $d = c/2$ = 6.37 Å, leads Sr_2RuO_4 to a 3D superconductor. It is this two-dimensional character of superconductivity of HTSC that makes its mixed state distinct from that in other layered superconductors.

Before discussing the origin of the second peak, let us concentrate on the observed anisotropy of the flux pinning. The linearity of initial increase in χ'' in the χ''-H curves (Fig. 15 (a) and Fig. 17 (a)) and the constancy of χ'' in the χ''-T curves (Fig. 19 (a)) with both H_{dc} // ab and H_{ac} // ab indicate that the dissipation is proportional to the number of flux lines along the ab planes and that the flux lines easily move along the ab planes without much magnetic impedance. On the other hand, even with H_{dc} // ab, the dissipation for H_{ac} // c is much less than that for H_{ac} // ab.

We first consider the shielding effect for H_{ac} in highly anisotropic superconductors as the origin of the anisotropic dissipation. Only when H_{ac} is along the c axis, the shielding current does not have the component along the c axis. Sr_2RuO_4 exhibits a large anisotropy in the critical currents: $J_{c,c}$ is at least two orders of magnitude smaller than $J_{c,ab}$ [2]. Therefore, the screening current against H_{ac} will much more easily exceed J_c for H_{ac} // ab, and results in dissipation. This interpretation semi-quantitatively agrees with the large dissipation for H_{ac} // ab and small dissipation H_{ac} // c. In addition, in this mechanism a dissipation in χ'' is expected to appear also for H_{dc} // c and H_{ac} // ab. In fact, some dissipation below $H_{c2//c}(T)$ is observed as shown in Fig. 16 (c), in contrast to much less dissipation below $H_{c2//c}(T)$ for H_{dc} // c and H_{ac} // c (Fig. 15 (b)). In order to confirm the shielding effect the measurements of the field dependence of the critical currents along both the ab planes and c axis may prove very useful.

Secondly, we will consider whether the 2D pinning mechanism reflecting its layered structure, the intrinsic pinning mechanism [48, 49], operates in Sr_2RuO_4. A theoretical criterion for the strictly working intrinsic pinning is that the coupling between the adjacent superconductive layers is negligible because of intermediating non-conducting layers, i.e. $\xi_c/d < 1$ [48]. This mechanism works well for HTSC, since this condition is satisfied except in the vicinity of T_c [50, 51]. On the other hand, ξ_c exceeds d by a factor of ~6 even at 0 K in Sr_2RuO_4, suggesting that the intrinsic pinning is probably very weak even if it exists. On the other hand, ξ_{GLc} exceeds d by factor of ~6 even at 0 K in Sr_2RuO_4. This means that the intrinsic pinning is probably very weak even if it exists. In fact, the modulation of the superconducting order parameter along the c axis between the conductive RuO_2 planes and the non-conductive SrO layers should be only by few percent. This is crudely estimated by

$$\Delta(d/2)=\Delta(0)\exp[-(d/2)^2/2\xi_{GLc}^2], \qquad (4.11)$$

where, $\Delta(z)$ is the superconducting order parameter as a function of the distance z from RuO_2 planes. Kwok *et al.* [50]. demonstrated, however, that the effectiveness of the intrinsic pinning persists in $YBa_2Cu_3O_{7-\delta}$ even near T_c where ξ_c is larger than d by a factor of 3. Therefore, it is not surprising that the intrinsic pinning is operating in Sr_2RuO_4 to some extent, in addition to the anisotropic shielding discussed in the previous paragraph.

Let us now discuss the origin of the peak effect in Sr_2RuO_4. We will argue below that the synchronization mechanism consistently explains the observed behavior in Sr_2RuO_4. But we first examine if other mechanisms apply to Sr_2RuO_4. The peak effect is observed only for H_{dc} // ab, so that the pancake vortices would not form in this field orientation. In addition, Sr_2RuO_4 is a 3D

superconductor, as mentioned above. Therefore, the 2D-3D crossover in the vortex structure is not relevant. In HTSC the flux melting is often responsible for the peak effects. When thermal fluctuations become sufficiently large, such that the mean-square displacement of a single vortex line is comparable to the lattice parameter of the vortex lattice, the system is expected to melt into a vortex liquid. Such a condition is often satisfied in HTSC because of the high T_c and short ξ, but is not likely to be satisfied in Sr_2RuO_4 with the low T_c and long ξ. For the melting transition, the characteristic field should vary as $(1-T/T_c)^m$ in the high temperature regime near T_c, valid for $H_{dc} // c$ [52], and vanishes just at T_c. Assuming that the relation is also valid for H_p in $H_{dc} // ab$, the H-T phase diagram of Sr_2RuO_4, as shown in Fig. 18, is not compatible with the flux melting. Because of frequency independence of $T(H_p')$ it is neither likely due to the depinning of vortices driven by the thermal activations, which is discussed also as the origin of the peak effects in HTSC [53].

A dissipation peak attributable to the skin effect appears when the superconducting penetration depth becomes comparable to the size of the sample. For this geometrical effect, the peak temperature depends logarithmically on frequencies of H_{ac} [54], as opposed to the observed $T(H_p')$ which is frequency independent. From the BCS formula for the penetration depth

$$\lambda(T)=\lambda(0)/[2(1-T/T_c)]^{1/2} \text{ valid for } T \approx T_c, \qquad (4.12)$$

the temperature at which $\lambda(T)$ is equal to the size of sample should be very close to T_c: $1-T/T_c \sim 4 \times 10^{-5}$ by using $\lambda_c(0) = 3.3 \times 10^4$ Å. Therefore, this mechanism cannot explain the second dissipation in Sr_2RuO_4. Here, we can also neglect the effect of a potential barrier of geometrical origin [55] because $H_{dc} // ab$ is along the planar surfaces of the plate-like sample.

Next we will consider two other possibilities for the origin of the peak effect, which is discussed for conventional superconductors [56], the matching and synchronization mechanism; the former is also discussed for HTSC [57]. Firstly, for a material with a periodic distribution of pinning centers, peak effects may occur when the vortex-lattice spacing matches the pinning-center spacing. This matching mechanism is immediately identifiable since the peaks should occur at a common value of the field regardless of the temperature. The large temperature dependence of H_p in Sr_2RuO_4 naturally eliminates this from the origin of the peak effect.

Now we will consider the synchronization mechanism [56], which is consistent with the peak effect of Sr_2RuO_4. If the flux-line lattice is nearly perfect, not all of the pinning centers can operate simultaneously. Therefore at low H_{dc} and low T, large dissipation can occur. The softening of the vortex lattice with increasing magnetic field and temperature will enable vortices

to synchronize with much more pinning centers and hence increase the bulk pinning force. The field characterizing this synchronization mechanism should be a function of both H_{dc} and T, as seen in Fig. 18, although it is difficult to evaluate $H_p(T)$ quantitatively. In addition, since the dissipation peak in this mechanism is not due to the hopping motions of the vortices between different metastable states, $T(H_p)$ is not the thermal activation type; consistent with the observed frequency independence shown in Fig. 21.

The collective pinning mechanism accompanied by the first order transition to the Fulde-Ferrell and Larkin-Ovchinnikov (FFLO) state has recently been discussed as the origin of the peak effect in $CeRu_2$ [58] and UPd_2Al_3 [59]. In these materials, the spin susceptibility χ_0 is so high to satisfy the paramagnetic limiting condition: $\chi_0 H_{c2}^2/2 > H_c^2/2\mu_0$ [60], where H_c is the thermodynamic critical field. In Sr_2RuO_4 with $\mu_0 H_c = 0.018$ T, $\chi_0 \sim 2 \times 10^{-4}$ m^{-3} is smaller by a factor of about three than that to satisfy this inequality. In addition, no hysteresis suggesting the first order transition is observed across H_p. Therefore, the FFLO state is not relevant to the observation in Sr_2RuO_4.

Quite recently, Rice and Sigrist [61] have suggested the possibility of the p-wave pairing state for the superconductivity of Sr_2RuO_4, which is the two-dimensional analog of the Balian-Werthamer (BW) state of ^{3}He. One might be tempted to associate the state below $H_p(T)$ in Fig. 18 with the presence of a different pairing state of the triplet pairing. However, even if p-wave pairing is indeed realized, a changeover between different representations of the triplet pairing as a function temperature at $H_{dc} = 0$ would not occur without a coexisting magnetic order. In fact the magnetic ordering has never reported in Sr_2RuO_4. Therefore, H_p does not represent the phase boundary between the different representations of the triplet pairing state, but represents the changeover in the vortex states.

5. Conclusion

We have investigated the superconducting and normal-state properties of Sr_2RuO_4, which is the only layered-perovskite superconductor without copper that is known so far, by measuring the dc-susceptibility and specific heat above T_c, the resistivity, and the ac-susceptibility under magnetic fields below 2 K using single crystalline Sr_2RuO_4.

In the normal state we found the T^2 dependence of the resistivity below 25 K, the enhanced paramagnetic spin susceptibility, and the enhanced Sommerfeld coefficient of the specific heat.

From the analyses in terms of the Willson ratio and Kadowaki-Woods ratio, these results are consistently described by the model of a strongly correlated system; the normal state of Sr_2RuO_4 is well characterized as a highly anisotropic Fermi liquid. The anisotropy is attributed to the highly anisotropic motion of the quasiparticles, reflecting the nearly two-dimensional electronic states. The coefficient of the T^2 term in the resistivity gives $m^*_c/m^*_{ab} \approx 550$, which agrees well with that calculated from the Fermi-surface parameters obtained from the quantum oscillations.

Concerning the peculiar temperature dependence of the resistivity along the c axis, we presented a systematic analysis based on a competition between the relaxation time of the quasiparticles for a number of scattering processes and the time required for the quasiparticles to move the interlayer distance d; in other words, the competition between the mean-free path along the c axis and d. However, it still remains unclear why the resistivity along the ab planes exhibits changeover in the temperature dependence at the same temperatures with that along the c axis. Further study is needed to clarify this mechanism by controlling the relaxation time, for example, by impurity substitution and by applied pressure.

From investigation of the upper critical fields H_{c2}, we showed that the superconducting state of Sr_2RuO_4 is also highly anisotropic with the ratio of the coherence lengths $\Gamma_S = \xi_{ab}(0)/\xi_c(0) = 26$. The ratio agrees well with the square root of the effective mass ratio in the normal state. Therefore, the superconductivity in Sr_2RuO_4 originates from Cooper pairs formed by the highly correlated electrons. In the sense that the coherence length along the c axis is much greater than the spacing between the adjacent RuO_2 planes, the superconductivity of Sr_2RuO_4 has three-dimensional character, rather than quasi-two dimensional character as in the high-T_c cuprate. In addition, the Ginzburg-Landau (G-L) parameters $\kappa(0) = 31$ ($H // ab$) and 1.2 ($H // c$) indicate that Sr_2RuO_4 is a type-II superconductor. The small $\kappa(0)$ value for $H // c$, however, indicates a soft type-II character.

We have discussed a peculiar anisotropic peak effect found in the layered perovskite superconductor without copper, Sr_2RuO_4. The peak effects are observed only when both the dc and ac magnetic fields are parallel to the ab planes, in contrast with those reported for the high-T_c cuprate superconductors. We argued that the anisotropic dissipation in χ'' of Sr_2RuO_4 is attributable to the highly anisotropic nature of superconductivity, reflecting the layered structure; in particular, the anisotropic critical current and possibly a minor contribution from the intrinsic flux-pinning. We also argued that the peak effects are ascribable to the synchronization mechanism.

Sr_2RuO_4 and HTSC share the layered perovskite structure and the highly anisotropic properties in the normal and superconducting states. On the other hand, a crucial difference between the two systems originates from the difference in dimensionality. The criterion for the dimensionality in the superconducting state is the ratio between the coherence length along the c axis ξ_c and the interlayer spacing d; the criterion in the normal state is the ratio between the mean-free path along the c axis l_c and d. The difference in the dimensionality of superconductivity results in the distinctive vortex dynamics of Sr_2RuO_4 from those of HTSC. In this respect, the highly anisotropic but 3D superconductivity of Sr_2RuO_4 serves as an ideal and important reference bridge between the anisotropic 2D superconductivity of HTSC and the less anisotropic conventional superconductivity in the study of flux dynamics. In addition, the three dimensionality in the normal state at low temperatures leads Sr_2RuO_4 to a highly anisotropic Fermi liquid. Therefore, Sr_2RuO_4 serves as an ideal reference material for investigation of the limits of applicability of the Fermi liquid theory to other highly correlated layered compounds, including high-T_c cuprates.

Acknowledgement

The author wishes to express his sincere thanks to Professor Toshizo Fujita for his stimulating discussion and encouragement through the course of this work. He is also grateful to Associate Professor Yoshiteru Maeno for fruitful discussion and advise. He wishes to express his appreciation to Dr. Tsutomu Nojima, Dr. Fumihiko Nakamura and Dr. Takasi Suzuki for helpful discussion and Dr. Frank Lichitenberg and Dr. J. Georg Bednortz for providing crystals. He is grateful to Dr. Andy P. Mackenzie for the beneficial collaboration. He acknowledges Mr. Shuji Nishizaki, growing high quality crystals, without which this study would not have been completed, Mr. Hiroaki Hashimoto for the greatest contribution to the discovery of superconductivity in Sr_2RuO_4, without which this work would not have been started, and Mr. Shin-ichi Ikeda for the excellent specific heat data. He acknowledges Professor Hironobu Fujii for allowing us to use a floating-zone furnace for the crystal growth. He thanks Dr. Masatune Kato for teaching in his early research days and his colleagues for help in his school life. Some of the measurements were performed at the Cryogenic Center of Hiroshima University. Last he very much appreciates his parents.

References

[1] J. G. Bednortz, K. A. Müller, Z. Phys. B **64** (1986) 189.

[2] Y. Maeno, H. Hashimoto, K. Yoshida, S. Nishizaki, T. Fujita, J. G. Bednortz and F. Lichtenberg, Nature **372** (1994) 532.

[3] R. J. Cava, B. Batlogg, K. Kiyono, H. Takagi, J. J. Krajewski, W. F. Peck, Jr., L. W. Rupp, Jr. and C. H. Chen, Phys. Rev. B **49** (1994) 11890.

[4] T. Oguchi, Phys Rev. B **51** (1995) 1385.

[5] A. P. Mackenzie, S. R. Julian, A. J. Diver, G. J. McMullan, M. P. Ray, G. G. Lonzarich, Y. Maeno, S. Nishizaki and T. Fujita, preprint (1995).

[6] L. F. Mattheiss, Phys. Rev. Lett. **58** (1987) 1028.

[7] I. H. Inoue, Y. Aiura, Y. Nishihara, Y. Haruyama, S. Nishizaki, Y. Maeno, T. Fujita, J. G. Bednortz and F. Lichtenberg, Proceedings of the 11th International Conference of Vacuum Ultraviolet Radiation Physics (VUV 11), Aug. 27~Sep. 1, 1995, Tokyo (to be published in J. Electr. Spectros. Relat. Phenom.).

[8] For example: H. Takagi, T. Ido, S. Ishibashi, M. Uota, S. Uchida and Y. Tokura, Phys. Rev. B **40** (1989) 2254.; Y. Ando, M. Sera, S. Yamagata, S. Kondoh, M. Onoda and M. Sato, Solid State Commun. **70** (1989) 303.

[9] For example: E. Zeldov, D. Majer, M. Konczykowski, V. B. Geshkenbein, V. M. Vinokur and H. Shtrikman, Nature **375** (1995) 373.; H. Pastoriza, M. F. Goffman, A. Arribére and F. de la Cruz, Phys. Rev. Lett. **72** (1994) 2951.; H. Safar, P. L. Gammel, D. A. Huse, D. J. Bishop, J. P. Rice and D. M. Ginsberg, Phys. Rev. Lett. **69** (1992) 824.

[10] H. Takagi, B. Batlogg, H. L. Kao, J. Kwo, R. J. Cava, J. J. Krajewski, W. F. Peck, Jr., Phys. Rev. Lett. **69** (1992) 2975.

[11] Y. Nakamura and S. Uchida, Phys. Rev. B **47** (1993) 8369.

[12] A. P. Mackenzie, S. R. Julian, D. C. Sinclair and C. T. Lin, preprint (1995).

[13] Y. Ando, G. S. Boebinger, T. Kimura and K. Kishio, preprint (1995)

[14] S. Uchida, private communications.

[15] D. G. Clarke, S. P. Strong and P. W. Anderson, Phys. Rev. Lett. **74** (1995) 4499.

[16] K. H. Fischer, Physica C **178** (1991) 161.

[17] F. Lichtenberg, A. Catana, J. Mannhart ang D. G. Schlom, Appl. Phys. Lett. **60** (1992) 1138.

[18] We acknowledge A. P. Mackenzie for the useful information.

[19] S. Nishizaki, Y. Maeno and T. Fujita, unpublished result.

[20] Y. Maeno, K. Yoshida, H. Hashimoto, S. Nishizaki, S. Ikeda, M. Nohara, T. Fujita, A. P. Mackenzie, N. E. Hussey, J. G. Bednortz and F. Lichtenberg, preprint (1995).

[21] The effective mass deduced from specific heat and quantum oscillations is essentially m^*_{ab} because of the topology of the Fermi surfaces of Sr_2RuO_4. We define m^*_c as $(v_{ab}/v_c)^2 m^*_{ab}/2$, which is useful to describe various physical quantities.

[22] P. W. Selwood, "*Magnetochemistry*" (Interscience Publishers. Inc. New York, 1956).

[23] M. E. Lines, J. Phys. Chem. Solids **31** (1970) 101.

[24] T. C. Leung, X. W. Wang and B. N. Harmon, Phys. Rev. B **37** (1988) 384.

[25] Measurements of C_P presented in this figure were performed by S. Ikeda.

[26] J. J. Neumeier, M. F. Hundley, M. G. Smith, J. D. Thompson, C. Allgeier, H. Xie, W. Yelon and J. S. Kim, Phys. Rev. B **50** (1994) 17910.

[27] K. Yamada, Prog. Theor. Phys. **53** (1975) 970.

[28] K. Kadowaki and S. B. Woods, Solid State Commun. **58** (1986) 507.

[29] K. Miyake, T. Matsuura and C. M. Varma, Solid State Commun. **71** (1989) 1149.

[30] Powder X-ray diffraction data were obtained by S. Nishizaki.

[31] Y. Inoue, M. Hara, Y. Koyama, Y. Maeno and T. Fujita, Proceedings of the 8th International Symposium on Superconductivity (ISS'95), Oct. 30 - Nov. 2, 1995, Hamamatsu, Japan (to be published in Advances in Superconductivity VIII (Springer-Verlag).).

[32] M. Udagawa, private communication.

[33] T. Vogt and D. J. Buttrey, Phys. Rev. B **52** (1995) R9843.

[34] N. Kumar and A. M. Jayannavar, Phys. Rev. B **45** (1992) 5001.

[35] K. Yoshida, Y. Maeno, S. Nishizaki and T. Fujita, to be published in Physica C.

[36] K. Yoshida, Y. Maeno, S. Nishizaki and T. Fujita, submitted to J. Phys. Soc. Jpn.

[37] A. M. Clogston, Phys. Rev. Lett. **9** (1962) 266.; B. S. Chandrasekhar, Appl. Phys. Lett. **1** (1962) 7.

[38] N. R. Werthamer, E. Helfand, P. C. Hohenberg, Phys. Rev. **147** (1966) 295.

[39] W. L. McMillan, Phys. Rev. **167** (1968) 331.

[40] S. Sakita, private communication.

[41] R. C. Morris, R. V. Coleman and R. Bhandari, Phys. Rev. B **5** (1972) 895.

[42] W. K. Kwok, J. A. Fendrich, C. J. van der Beek and G. W. Crabtree, Phys. Rev. Lett. **73**

(1994) 2614.

[43] K. Kishio, J. Shimoyama, Y. Kotaka and K. Yamafuji, Proc. 7th Int. Workshop on Critical Currents in Supercond. ed. by H. W. Weber (World Scientific 1994) p. 339.

[44] S. Bhattacharya and M. J. Higgins, Phys. Rev. Lett. **70** (1993) 2617.

[45] S. Bhattacharya and M. J. Higgins, Phys. Rev. B **49** (1994) 10005.

[46] H. Ito, M. Watanabe, Y. Nogami, T. Ishiguro, T. Komatsu, G. Saito and N. Hosoito, J. Phys. Soc. Jpn. **60** (1991) 3230.

[47] H. Ito, J. Phys. Soc. Jpn. **64** (1995) 3018.

[48] M. Tachiki and S. Takahashi, Solid State Commun. **70** (1989) 291.

[49] P. H. Kes, J. Aarts, V. M. Vinokur and C. J. van der Beek, Phys. Rev. Lett. **64** (1990) 1063.

[50] W. K. Kwok, U. Welp, V. M. Vinokur, S. Fleshler, J. Downey and G. W. Crabtree, Phys. Rev. Lett. **67** (1991) 390.

[51] T. Hanaguri, T. Fukase, I. Tanaka and H. Kojima, Phys. Rev. B **48** (1993) 9772.

[52] A. Houghton, R. A. Pelcovits and A. Sudbø, Phys. Rev. B **40** (1989) 6763.

[53] A. Gupta, P. Esquinazi, H. F. Braun and H.-W. Neumüller, Phys. Rev. Lett. **63** (1989) 1869.

[54] V. B. Geshkenbein, V. M. Vinokur and R. Fehrenbacher, Phys. Rev. B **43** (1991) 3748.

[55] E. Zeldov, A. I. Larkin, V. B. Geshkenbein, M. Konczykowski, D. Majar, B. Khaykovich, V. M. Vinokur and H. Shtrikman, Phys. Rev. Lett. **73** (1994) 1428.

[56] A. M. Campbell and J. E. Evetts, Adv. Phys. **21** (1972) 199.

[57] G. Yang, P. Shang, S. D. Sutton, I. P. Jones, J. S. Abell and C. E. Gough, Phys. Rev. B **48** (1993) 4054.

[58] H. Goshima, T. Suzuki, T. Fujita, M. Hedo, T. Nakama and K. Yagasaki, PhysicaB 206&207 (1995) 193.

[59] K. Gloos, M. Modler, H. Schimansky, C. D. Bredl, C. Geibel, F. Steglich, A. I. Buzdin, N. Sato and T. Komatsubara, Phys. Rev. Lett. **70** (1993) 501.

[60] This inequality is obtained based on the equation (4.1), $\chi_0 = 2\mu_B N(\varepsilon_F)$ and the BCS rerations $\Delta/k_B T_c = 1.76$ and $\Delta^2 N(\varepsilon_F)/2 = H_c^2/2\mu_0$, where Δ is the superconducting gap parameter.

[61] T. M. Rice and M. Sigrist, preprint (1995).

	α(hole-like)	β(electron-like)	γ(electron-like)
frequency F (kT)	3.05	12.7	18.5
Fermi wave number k_F (Å^{-1})	0.302	0.621	0.750
dispersion $\Delta k_F/k_F$ (%)	0.21	1.3	< 0.9
cyclotron mass m^* (m_e)	3.4	6.6	12.0
carrier number n (per Ru)	0.26	0.91	1.33
hopping matrix element t_c (K)	1.2	17	< 9
Fermi velocity v_{ab} (m/s)	1.0×10^5	1.1×10^5	7.2×10^4
v_c (m/s)	2.9×10^2	4.0×10^3	2.1×10^3
transfer rate $1/\tau_c$ (s^{-1})	4.5×10^{11}	6.3×10^{12}	3.4×10^{12}

Table 1. The Fermi-surface parameters of Sr_2RuO_4 determined from the quantum oscillations and some derived quantities. The three nearly cylindrical Fermi surfaces are labeled as α, β and γ.

			along *ab*	along *c*
critical temperature	T_c	(K)	0.9	
upper critical field	$\mu_0 H_{c2}(0)$	(T)	0.78	0.030
coherence length	$\xi_{GL}(0)$	(Å)	1.05×10^3	40
Fermi velocity	v_{ab}, v_c	(m/s)	6.9×10^4	2.6×10^3
thermodynamic critical field	$\mu_0 H_{c0}(0)$	(T)	0.018	
lower critical field	$\mu_0 H_{c1}(0)$	(T)	1.4×10^{-3}	2.8×10^{-3}
penetration depth	$\lambda(0)$	(Å)	1.3×10^3	3.3×10^4
G-L parameter	$\kappa(0)$		31	1.2

Table 2 Anisotropic superconducting parameters of Sr_2RuO_4. The underlined quantities were directly measured, and the others were estimated using theoretical relations.

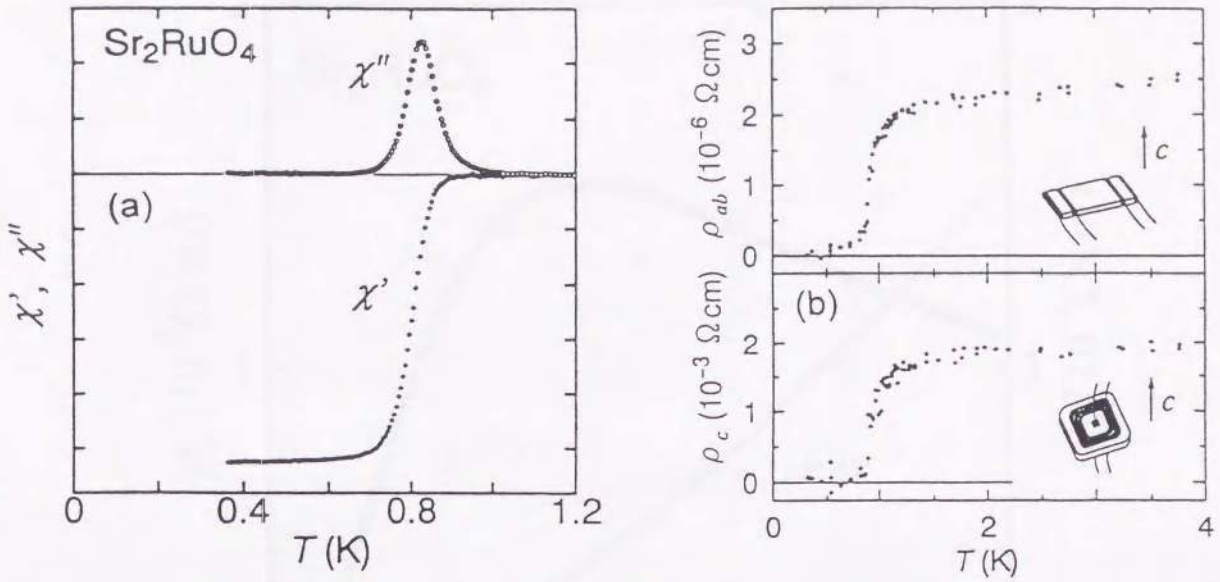

Fig. 1 (a) The ac susceptibility of a single crystal of Sr_2RuO_4 measured by a mutual-inductance method at a magnetic field of $H_{ac} = 0.67$ Oe parallel to the c axis, and at a frequency of 1000 Hz. Top, χ'' (imaginary part); bottom, χ' (real part).
(b) The anisotropic resistivity of Sr_2RuO_4 below 4 K. Insets, attachment of the electrodes.

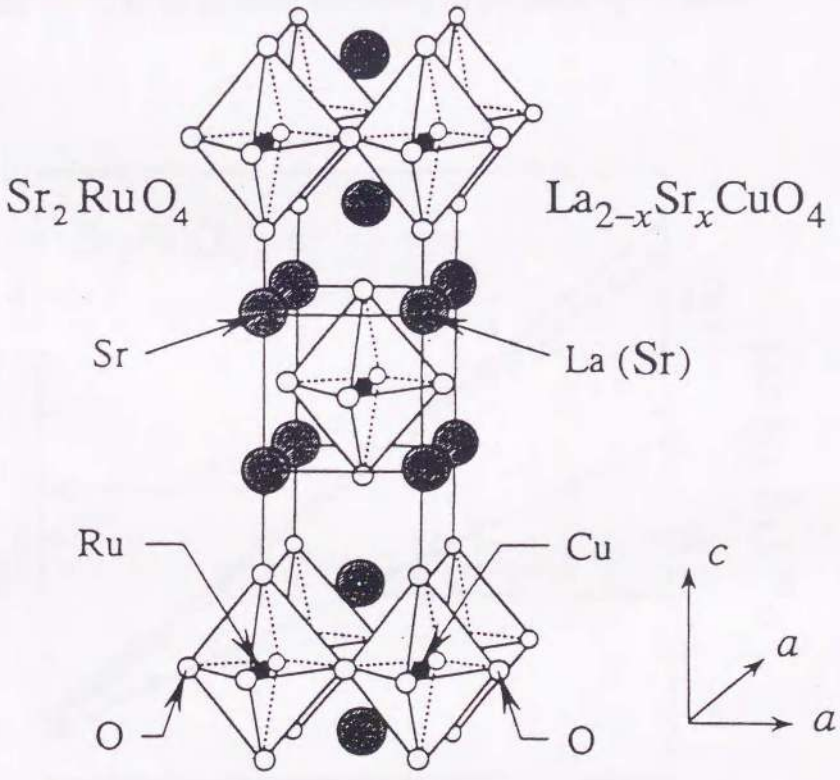

Fig. 2 Schematic crystal structure of superconductors Sr_2RuO_4 and $La_{2-x}Sr_xCuO_4$. Also shown are the directions of the tetragonal principal axes. ($b = a$ in a tetragonal structure.)

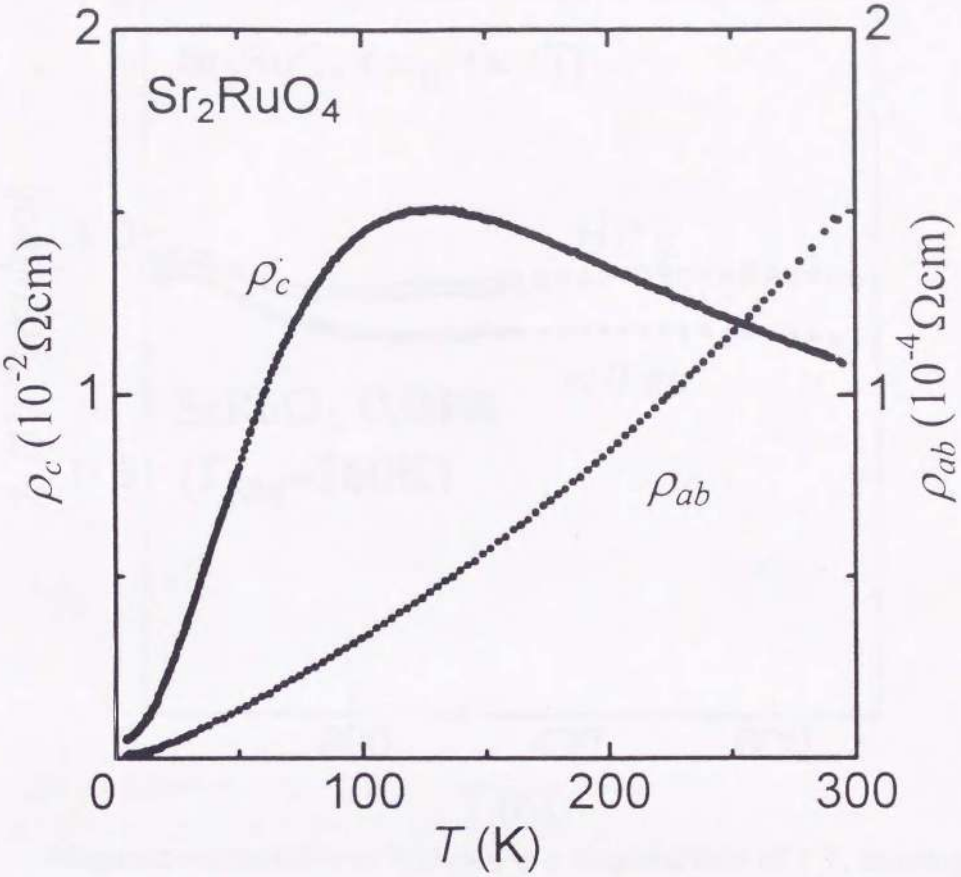

Fig. 3 The anisotropic resistivity of Sr_2RuO_4 up to 300 K.

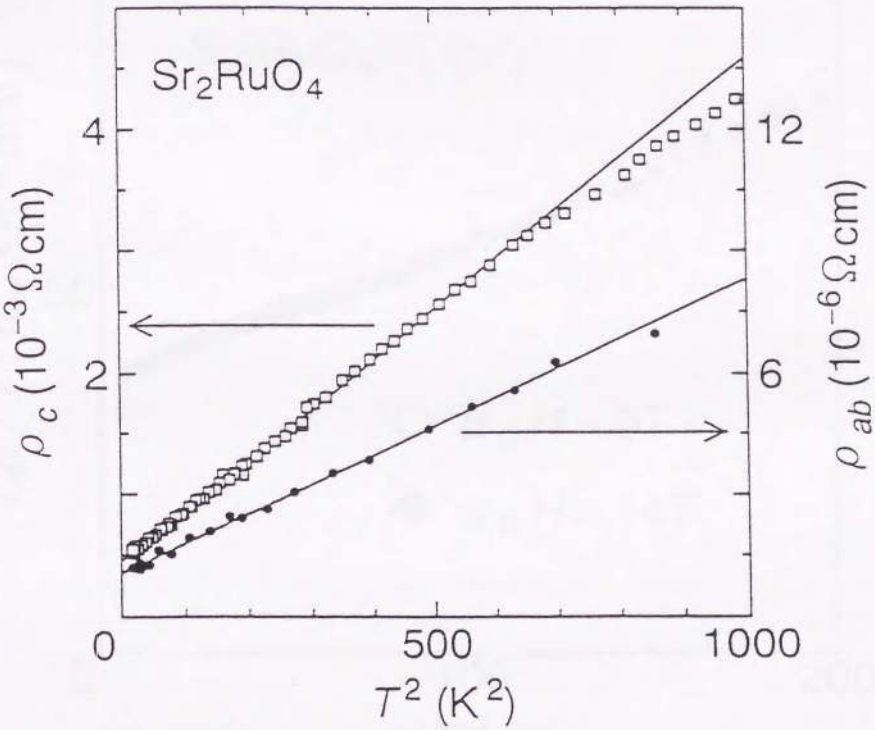

Fig. 4 The resistivities along the *ab* planes (ρ_{ab}) and the *c* axis (ρ_c) plotted against T^2. The solid lines represent the fits below 25 K: $\rho = \rho_0 + AT^2$.

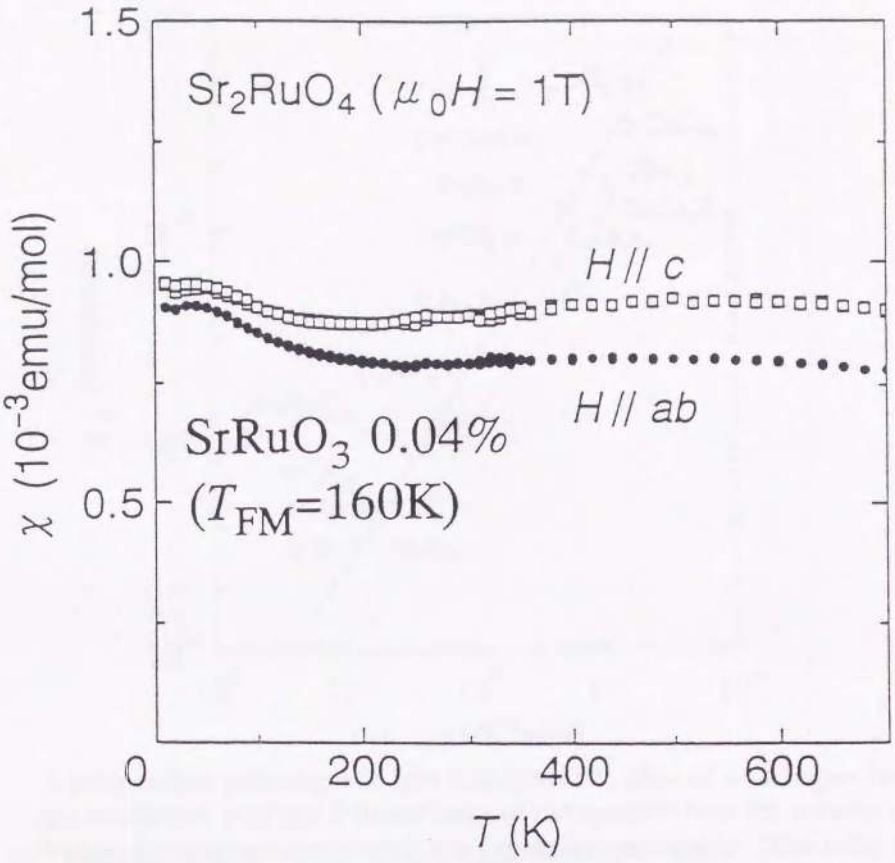

Fig. 5 Magnetic susceptibility of Sr_2RuO_4 in a magnetic field of 1 T, showing very weak temperature dependence up to 700 K. Data have been corrected for a diamagnetic contribution from the core electrons of - 0.91 × 10^{-4} emu/mol.

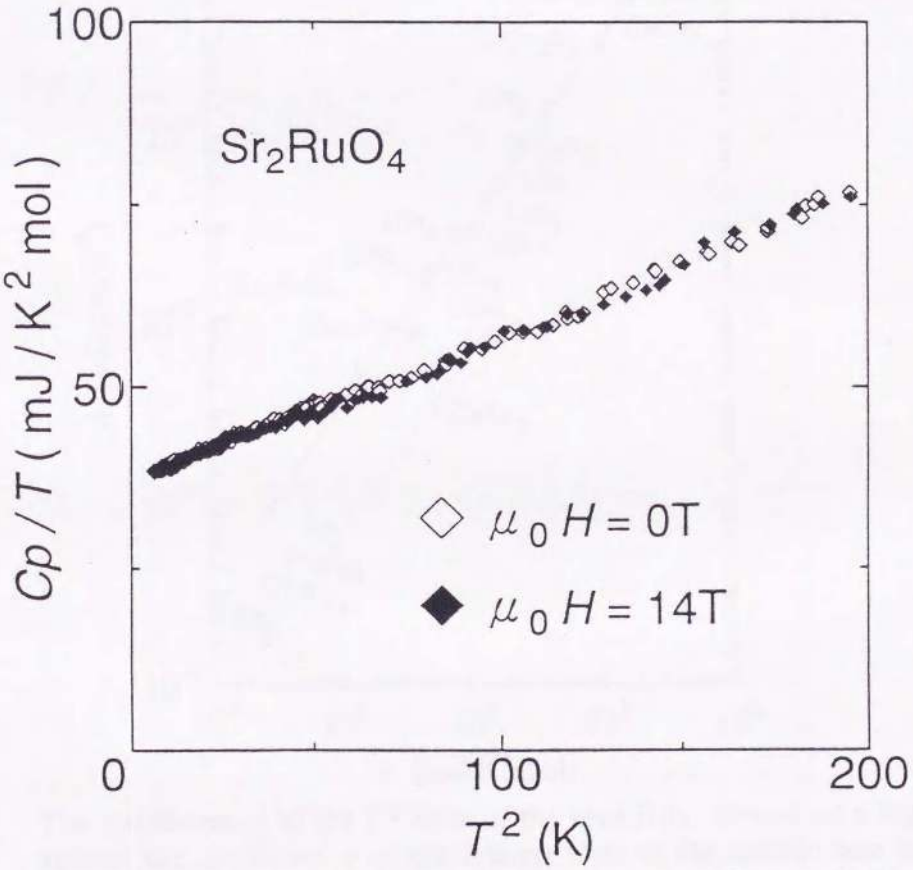

Fig. 6 The specific heat divided by temperature, C_p/T, against T^2 for a single crystal in zero field and under a magnetic field of 14 T along the *c* axis.

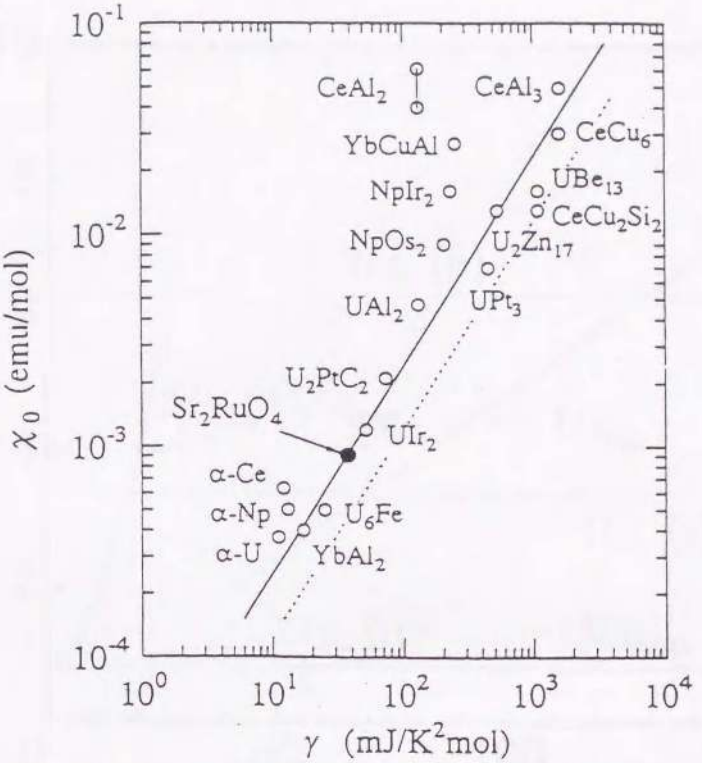

Fig. 7 T-independent paramagnetic spin susceptibility, plotted on a logarithmic scale against the coefficient γ of the T-linear term of the specific heat for a variety of compounds. Values for uranium compounds are expressed per mol-U. The solid and broken lines represent the Wilson ratio $R_W = 2$ and 1, respectively.

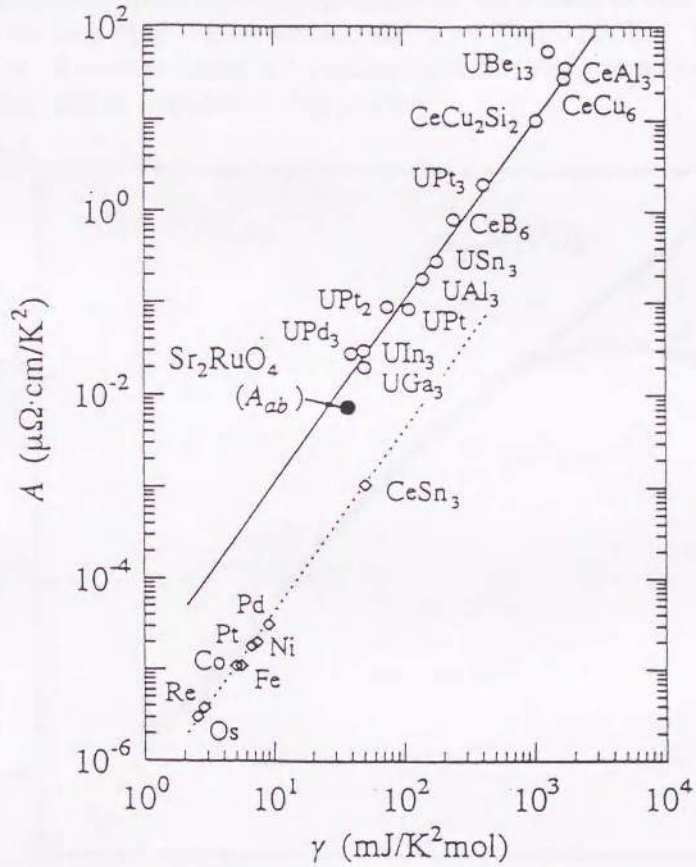

Fig. 8 The coefficient A of the T^2 term of the resistivity, plotted on a logarithmic scale against the coefficient γ of the T-linear term of the specific heat for a variety of compounds. The solid and broken lines represent the Kadowaki-Woods ratio $A/\gamma^2 = a_0 = 1.0 \times 10^{-5}$ $\mu\Omega$cm/(mJ/Kmol)^2 and $a_0/25$, respectively.

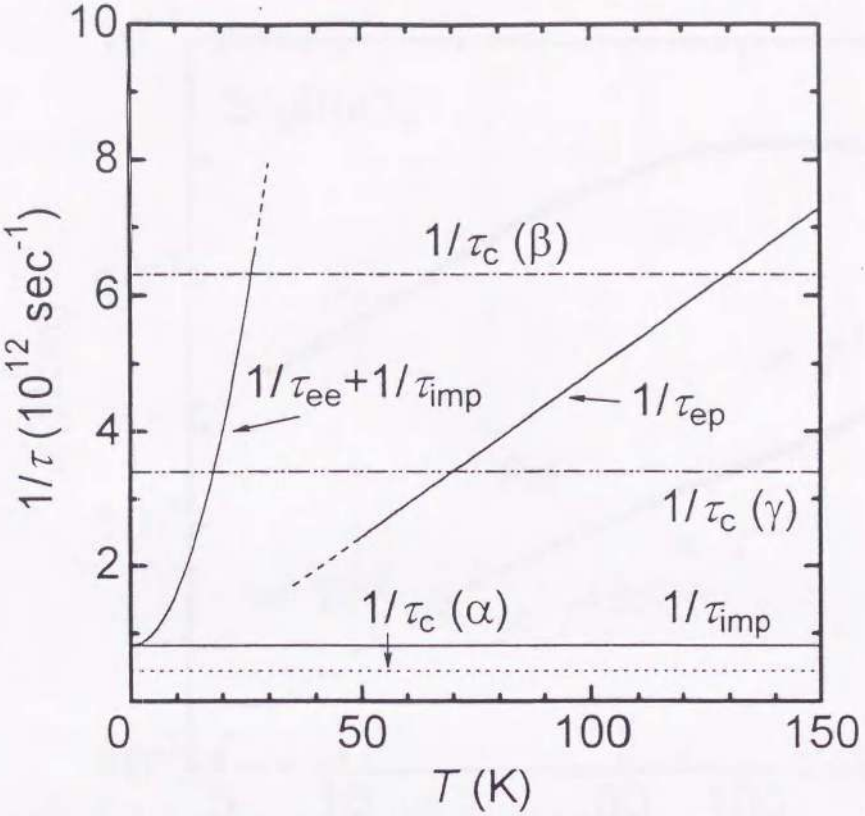

Fig. 9 Schematic temperature dependence of the inverse relaxation time of quasiparticle for a number of scattering processes and the inverse characteristic time $1/\tau_c$ for the quasiparticle to move interlayer distance for each band at low temperature. (a) for α-Fermi surface, (b)β-Fermi surface and (c) γ-Fermi surface. Here, τ_{ee}, τ_{ep} and τ_{imp} are the relaxation times of quasiparticle for the scattering by quasiparticles, by phonons and by impurities, respectively.

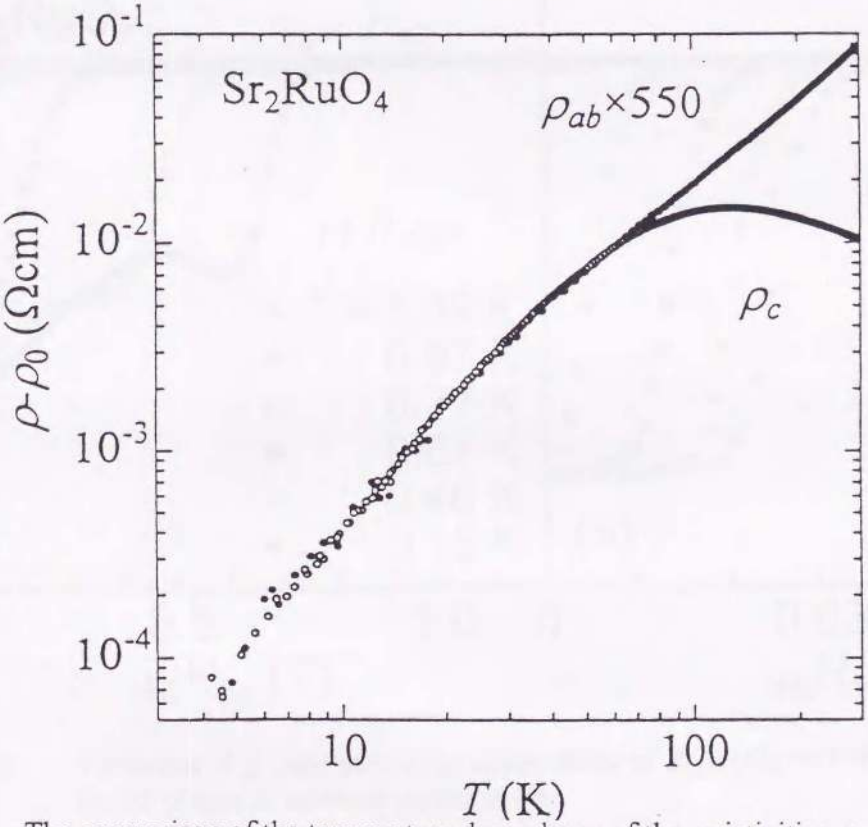

Fig. 10 The comparison of the temperature dependence of the resistivities ρ_{ab} and ρ_c, plotted on a logarithmic scale. ρ_{ab} is multiplied by 550 (= A_c/A_{ab}) to simplify the comparison.

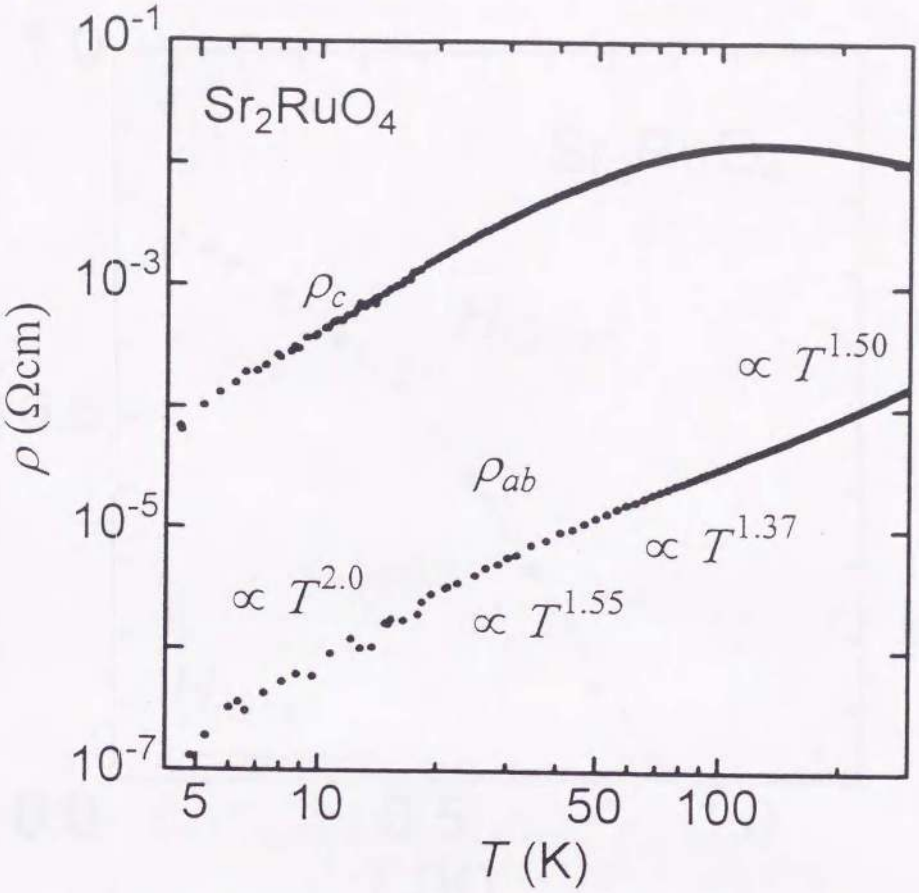

Fig. 11 The anisotropic resistivity plotted on a logarithmic scale.

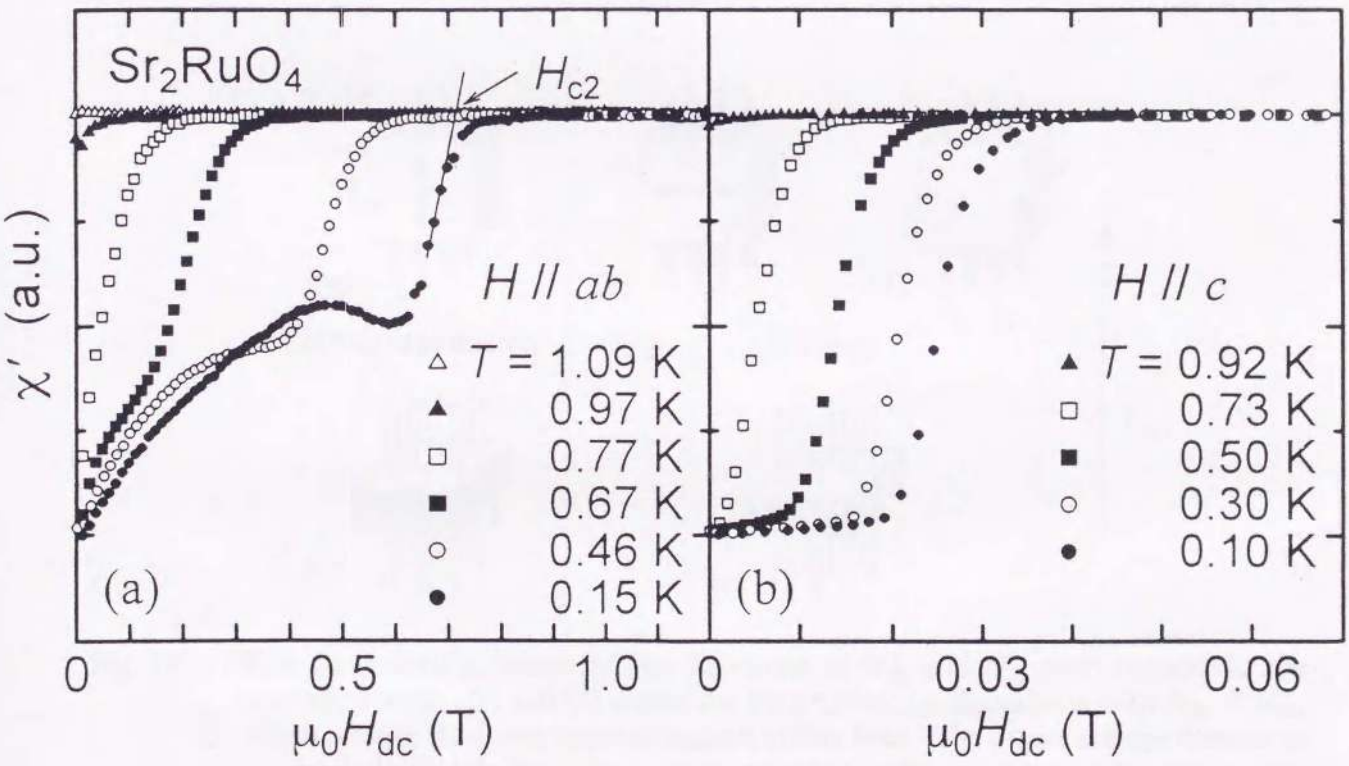

Fig. 12 Variations of χ' (real part) of ac susceptibility of Sr_2RuO_4 with the dc field H_{dc} along the *ab* planes at selected temperatures.

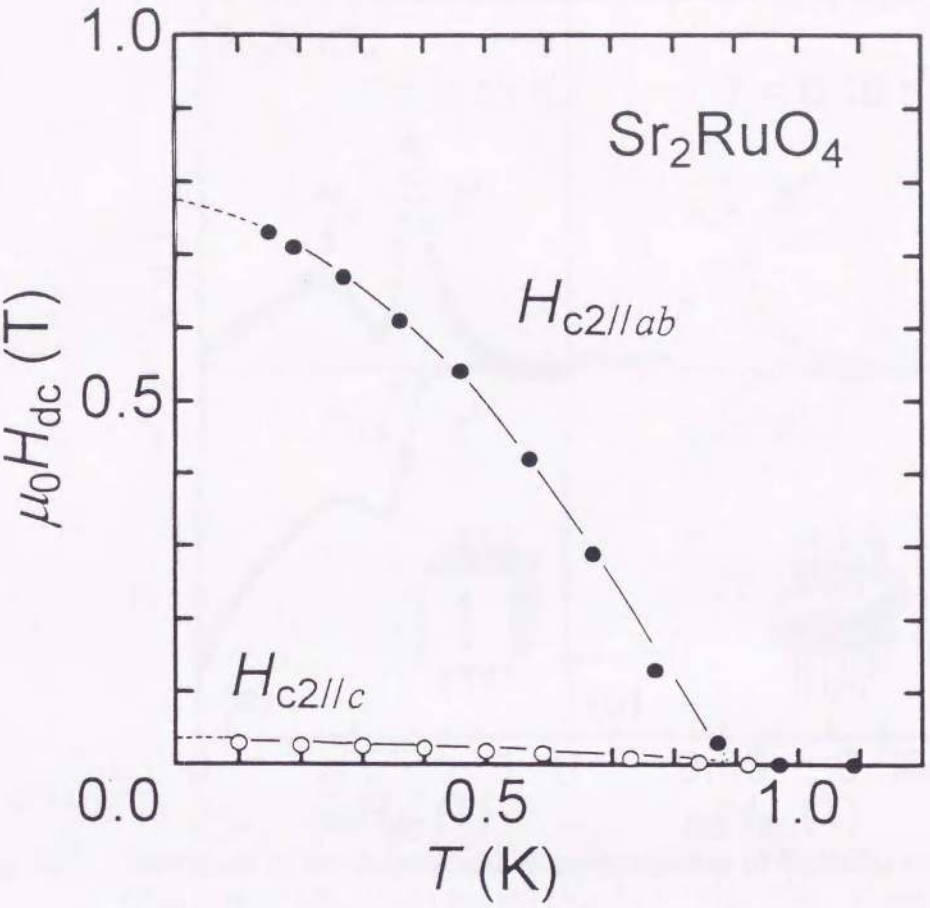

Fig. 13 Variations of the upper critical fields H_{c2} with temperature.

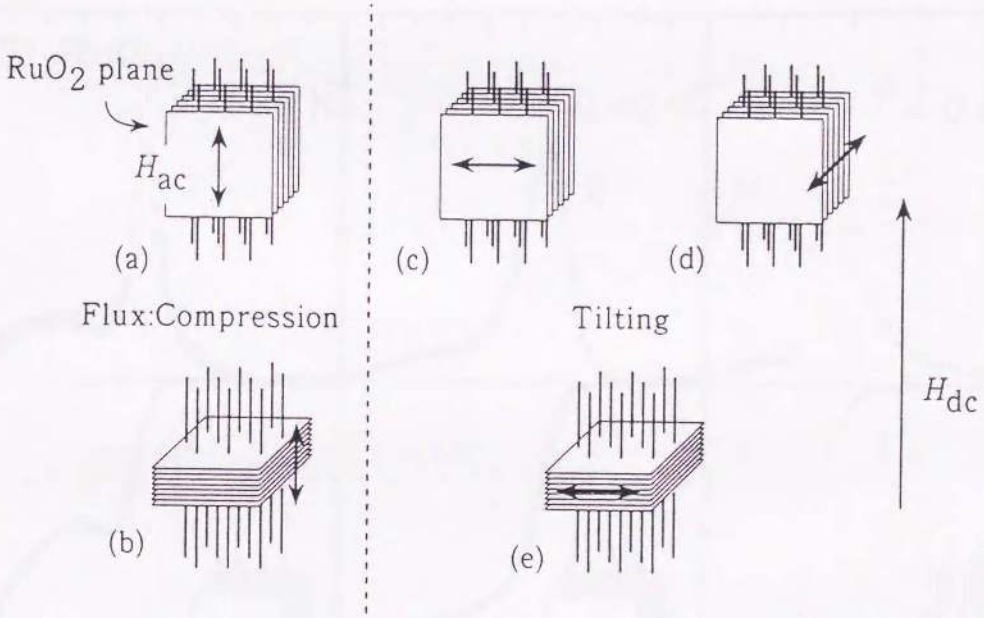

Fig. 14 Five basic configurations of the directions of H_{dc} and H_{ac} with respect to the crystalline axes. (a) and (b) depict the longitudinal configurations with H_{dc} // H_{ac}, which provide the compressional motion of flux lines. The others are the transverse configurations with $H_{dc} \perp H_{ac}$, which provide the tilting motion of flux lines. The stacking of RuO_2 planes, flux lines and the directions of H_{ac} are sketched by the planes, lines and arrows, respectively.

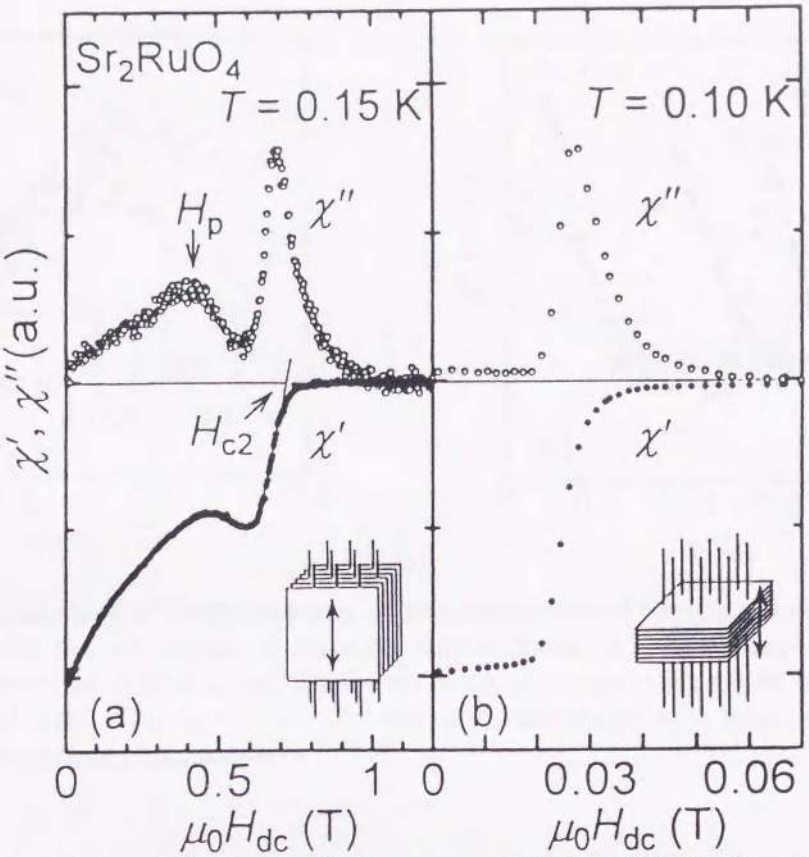

Fig. 15 Variations of the longitudinal ac susceptibilities of Sr_2RuO_4 with the dc field. (a) (H_{dc} // ab) // (H_{ac} // ab) and (b) (H_{dc} // c) // (H_{ac} // c). χ' and χ'' are the real and imaginary components of the ac susceptibility. The ac fields of $\mu_0 H_{ac}$ = 7 μT (//ab) and 3 μT (// c) at a frequency of 1000 Hz were used.

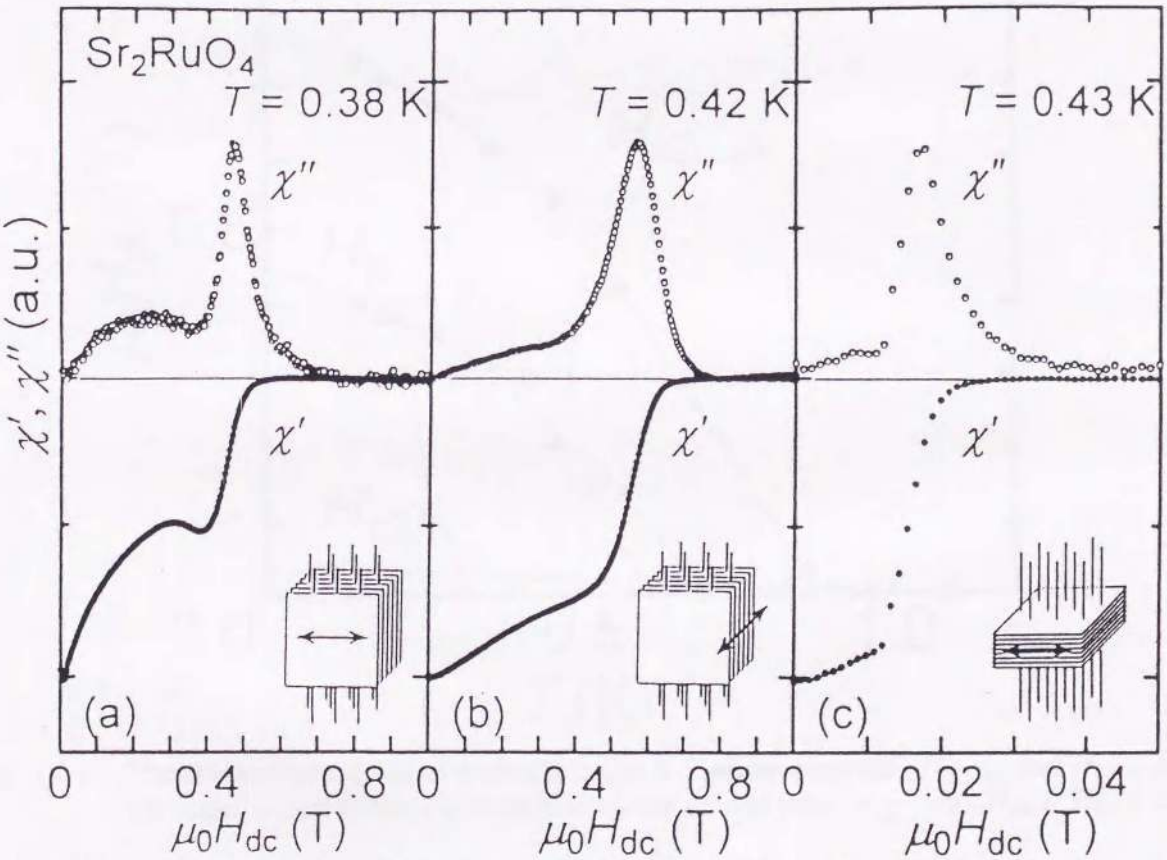

Fig. 16 Variations of the transverse ac susceptibilities of Sr_2RuO_4 with the dc field. (a) (H_{dc} // ab) ⊥ (H_{ac} // ab), (b) (H_{dc} // ab) ⊥ (H_{ac} // c) and (c) (H_{dc} // c) ⊥ (H_{ac} // ab). The ac field used is $\mu_0 H_{ac}$ = 15 μT.

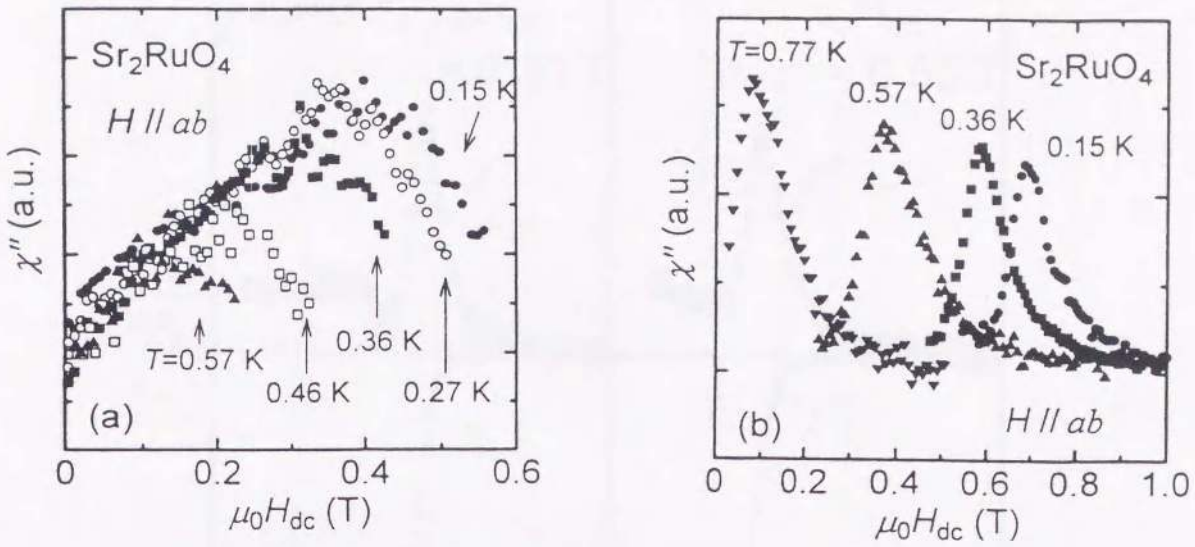

Fig. 17 Variations of χ'' (imaginary part) of ac susceptibility of Sr_2RuO_4 with the dc field H_{dc} along the *ab* planes at selected temperatures; (a) the variation of the second dissipation with H_{dc} and (b) the variation of the first dissipation with H_{dc}. The ac field used is $\mu_0 H_{ac} = 7\ \mu T$. All the curves are scaled with each other and valid for quantitative comparison.

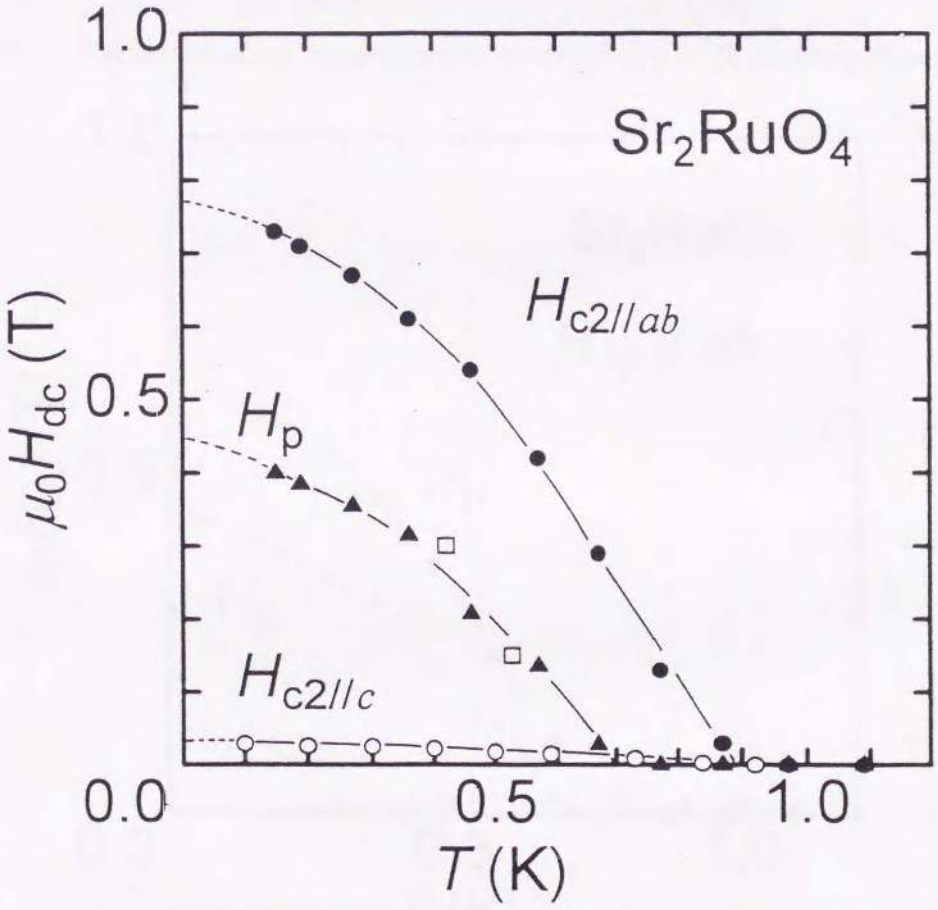

Fig. 18 The characteristic fields of Sr_2RuO_4 in the *H-T* phase diagram. $H_{c2//ab}$ and $H_{c2//c}$ are the upper critical fields; H_p is defined by the second peak in χ'' with H_{dc} // H_{ac} // *ab*.

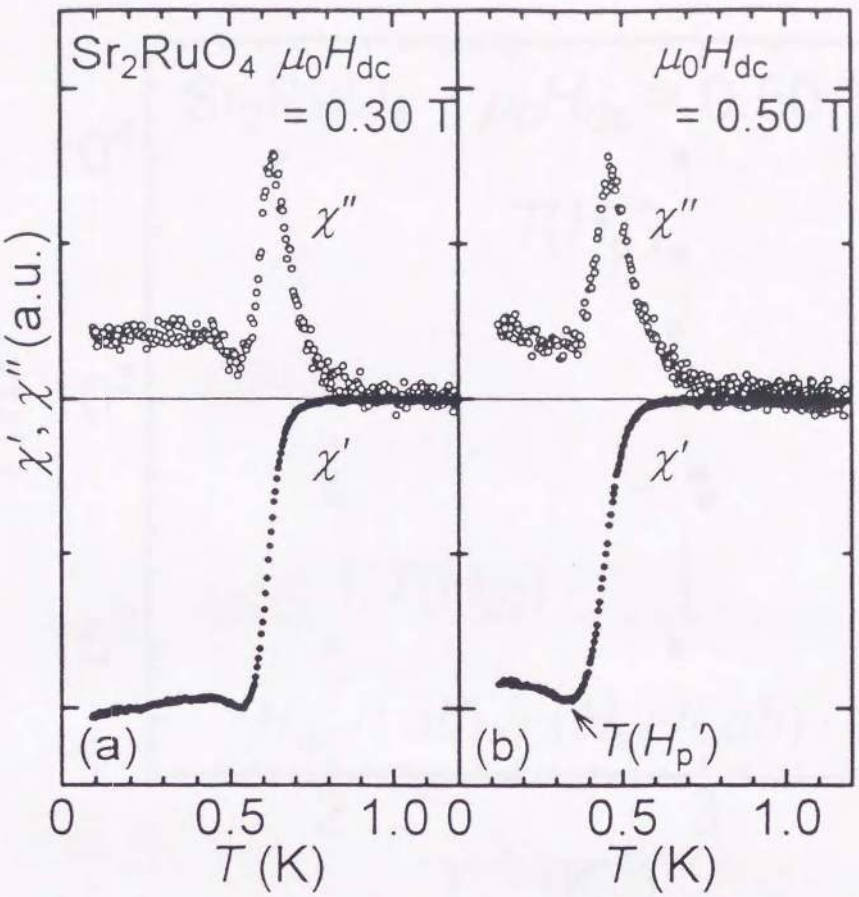

Fig. 19 Variations of the longitudinal ac susceptibility of Sr_2RuO_4 with temperature.

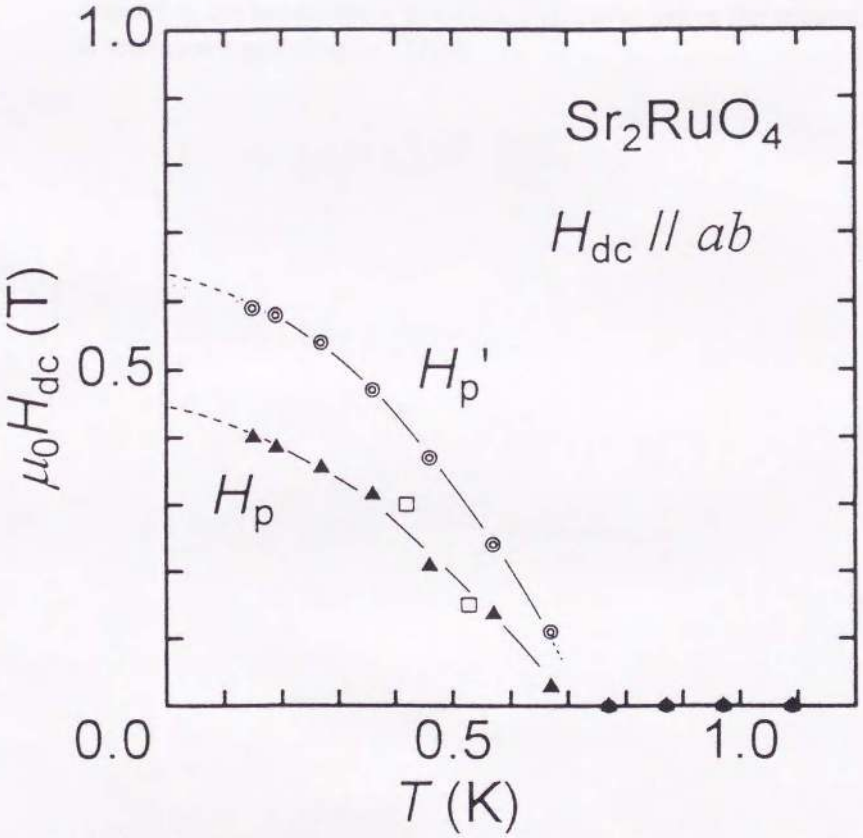

Fig. 20 Variations of H_p and H_p' with temperature. H_p' is defined by the field at which χ' - H curve takes a minimum.

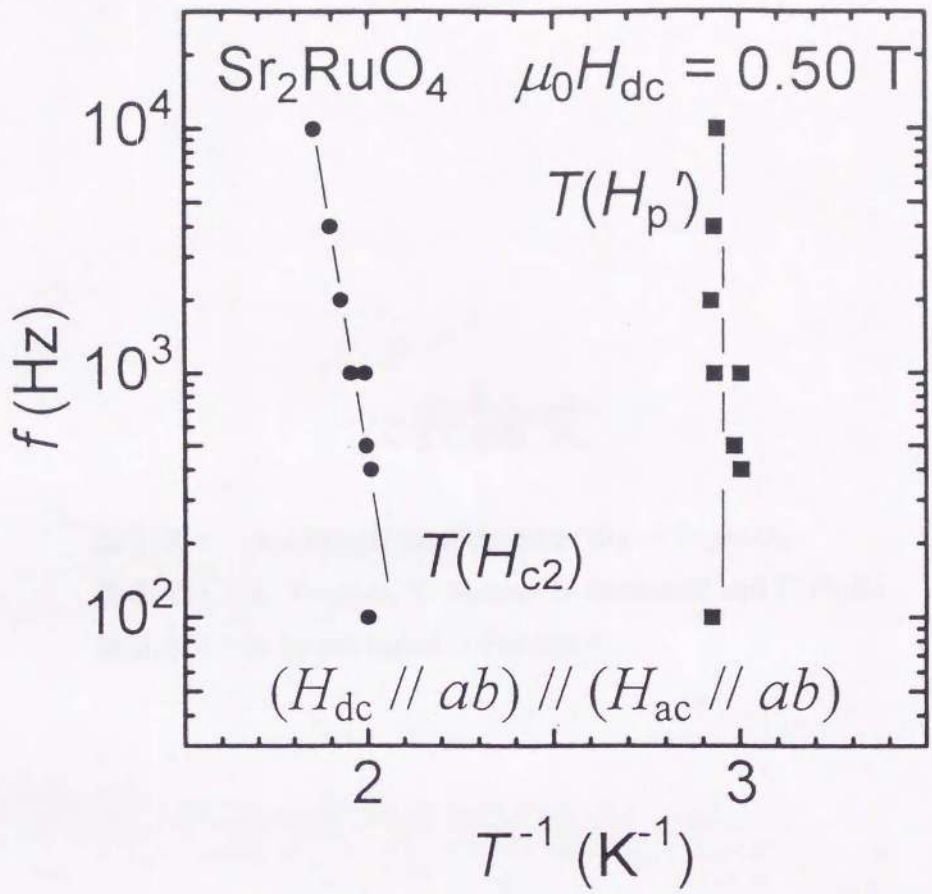

Fig. 21 The frequency dependence of $T(H_{c2})$ and $T(H_p')$ at $\mu_0 H_{dc} = 0.50$ T. Here $T(H_p')$ is defined as the temperature at which χ'-T curve takes the minimum (Fig. 7 (b)), which is well corresponding to $T(H_p)$.

公表論文

論文名： Anisotropic superconductivity of Sr_2RuO_4

著者名： K. Yoshida, Y. Maeno, S. Nishizaki and T. Fujita

雑誌名： to be published in Physica C.

参考論文

1 論文名： Superconductivity in layered perovskaite without copper
著者名： Y. Maeno, H. Hashimoto, K. Yoshida, S. Nishizaki, T. Fujita, J. G. Bednorz and F. Lichtenberg
雑誌名： Nature 372 (1994) 532-534.

2 論文名： Ion-Size Effects on the Structure and Superconductivity of La-214 compounds at 1/8 doping
著者名： K. Yoshida, F. Nakamura, Y. Tanaka, Y.Maeno and T. Fujita
雑誌名： Physica C 230 (1994) 371-377.

3 論文名： Effects of Ionic Size on the x = 1/8 Anomaly in $La_{2-x}Ba_{x-y}M_yCuO_4$ (M = Ca, Sr)
著者名： K. Yoshida, F. Nakamura, Y. Tanaka, Y. Maeno, T. Kagayama, G. Oomi and T. Fujita
雑誌名： Physica B 194-196 (1994) 2051-2052.

4 論文名： Stability of Low-Temperature Tetragonal Phase in $La_{2-x}Ba_xCuO_4$ and Related Compounds
著者名： F. Nakamura, K. Yoshida, Y. Tanaka, X. Z. Bao, Y. Maeno and T. Fujita
雑誌名： Journal of Superconductivity 7 (1994) 33-35.

5 論文名： Superconductivity and Structural Phase Transition in $La_{2-x}Ba_xCuO_4$ with La Partially Replaced by Th
著者名： X. Z. Bao, Y. Maeno, Y. Tanaka, K. Yoshida and T. Fujita
雑誌名： Advances in Superconductivity VI (1993) 375-378.

6 論文名： Magnetic and Transport properties of $La_{2-x}Sr_xCuO_4$ near x = 1
著者名： F. Nakamura, K. Yoshida, K. Sugiyama, Y. Maeno and T. Fujita
雑誌名： Physica C 185-189 (1991) 1103-1104.

7 論文名： Simple and Reliable Method for Determination of Oxygen Content in High—T_c Copper Oxides

著者名： Y. Maeno, H. Teraoka, K. Matsukuma, K. Yoshida, K. Sugiyama, F. Nakamura and T. Fujita

雑誌名： Physica C 185-189 (1991) 587-588.